IMAGING DOSE DURING THE RADIOTHERAPY PROCESS

Tebogo Daniel Baloyi

A research report submitted to the Faculty of Science, University of the Witwatersrand, Johannesburg, in partial fulfillment of the Degree of Master of Science in Physics in the field of Medical Physics.

Johannesburg, 2018.

DECLARATION

I declare that this research report is my own unaided work. It is being submitted for the degree of Master of Science in the University of the Witwatersrand, Johannesburg. It has not been submitted before for any degree or examination in any other University.

This study received an ethics clearance from the Human Research Ethics Committee of the University of the Witwatersrand (no. M 160825).

Student Name: Tebogo Daniel Baloyi

Student Number: 1313530

Signature: 

Date: 05 February 2018

ABSTRACT

OBJECTIVES: This study aimed to investigate the total concomitant imaging dose accumulated from different imaging modalities during the radiotherapy process. The radiation dose resulting from imaging modalities is often neglected because it is viewed as too low compared to high levels of radiation dose normally prescribed for treatment. With recent advances in high dose imaging technology integrated into radiotherapy treatment units, there has been a growing concern regarding the imaging dose as a result of their increased use.

DESIGN & METHOD: The study was conducted at the Charlotte Maxeke Johannesburg Academic Hospital (CMJAH) and Richards Bay Medical Institute (RBMI). Imaging modalities investigated at CMJAH were fluoroscopy simulation, Computed Tomography (CT) scanning and MV planar imaging. Imaging modalities investigated at RBMI were kV Cone Beam CT, CT scanning and kV planar imaging. CT dosimetry was performed using a head and body phantom with a pencil ionisation chamber. A calibrated parallel plate diagnostic ionisation chamber with a 30 × 30 cm^2 acrylic phantom was used for the fluoroscopy simulator and kV planar imaging dosimetry. The total imaging dose was estimated as the sum of dose resulting from each modality taking into account the number of times imaging was performed, on 20 patients from each institution.

RESULTS:

CMJAH: The measured volume Computed Tomography Dose Index ($CTDI_{vol}$) was 17.98 ± 1.54 mGy and 20.26 ± 1.64 mGy for head and body scanning protocols respectively. The measured simulator Entrance Surface Air Kerma (ESAK) dose from pelvic imaging protocol for 20 patients of different sizes ranged from 0.16 ± 0.01 mGy to 0.32 ± 0.03 mGy for anterior-posterior/posterior-anterior (AP/PA) projections and 1.49 ± 0.13 mGy to 3.18 ± 0.27 mGy for lateral projections. The total dose accumulated during the complete course of treatment from MV portal imaging ranged from 5 cGy to 43 cGy for both AP/PA and lateral projections. The average estimated effective doses to patients resulting from a single planning CT procedure, acquisition of one pair of AP/PA and lateral simulation films and one session of 6 MV portal imaging verification were 7.57 ± 0.61 mSv, 0.19 ± 0.02 mSv and 4.80 ± 0.24 mSv respectively. Based on a series of 20 patients,

the calculated average effective dose accumulated during a complete course of treatment were 7.53 ± 0.61 mSv, 0.37 ± 0.03 mSv and 15.53 ± 0.78 mSv respectively from each modality respectively. The greatest contribution to the patient's total effective dose from imaging alone originated from the planning CT scan. However when taking into account the number of imaging procedures typically prescribed for each modality, the 6 MV portal imaging contributed the highest dose.

RBMI: The measured $CTDI_{vol}$ was 79.60 ± 6.61 mGy and 33.79 ± 2.80 mGy for the head and body scanning protocols respectively. For kVCBCT, the $CTDI_{vol}$ measured was 5.20 ± 0.43 mGy and 14.40 ± 1.19 mGy for the head and body scanning protocols respectively. The ESAK measured for kV planar imaging of the head was 0.31 ± 0.03 mGy and 0.12 ± 0.01 mGy for the AP/PA and lateral projections respectively. For AP/PA pelvic imaging the ESAK ranged from 0.16 ± 0.01 mGy to 0.33 ± 0.03 mGy for small to extra-large patients. For lateral imaging the range was 1.49 ± 0.13 mGy to 3.18 ± 0.27 mGy from small to extra-large patients respectively. The estimated average effective dose to 20 patients resulting from the planning CT, kVCBCT and kV portal imaging procedures during the complete course of treatment were approximately 19.96 ± 1.66 mSv, 11.82 ± 0.98 mSv and 1.49 ± 0.12 mSv respectively. The greatest contribution to the total effective dose from imaging alone originated from the planning CT scan.

CONCLUSION: The results indicate that considerable dose could be delivered to patients during image guided radiotherapy, primarily when imaging procedures are over utilized and not optimized, adding more burden of dose to the already high levels of dose they receive from their treatment. The dose contribution from the planning CT was the highest and is influenced primarily by the scan length and the number of examinations. This can be reduced if scans are not acquired beyond the region of interest (ROI) required for planning purposes or by adjusting protocols to larger slice spacing outside the ROI.

Inadequate scanning of patients can also add more dose to patients if the CT examination is repeated to acquire sufficient image information required for radiation therapy planning. Modern imaging techniques such as kVCBCT applied during patient setup verification, can also add a significant dose when prescribed to confirm setup on a daily basis. kV planar imaging dose was significantly lower than all other imaging modalities

researched in this study. Compared with MV planar imaging, the average effective dose to the patient during the complete course of treatment from MV portal imaging was 7.95 ± 0.65 mSv whereas it was 1.49 ± 0.13 mSv from kV portal imaging. Therefore, if the soft tissue image information from MV planar imaging is not justified, kV imaging is recommended. On the other hand, single exposure MV imaging of static treatment ports could be subtracted from the prescribed radiotherapy dose.

DEDICATION

Dedicated to the Lord Almighty God himself, for the strength, wisdom, knowledge and guidance He gave me throughout my studies and everyday life, my sons (Excellent and Gosego), brothers and sisters, and also in loving memory of my beloved parents, Thomas and Rosina Baloyi.

ACKNOWLEDGEMENTS

Firstly, I would like to thank my supervisor Prof Debbie van der Merwe, her guidance and commitment to highest standards continues to inspire and motivate me academically.

In addition, I would also like to acknowledge the contribution of Mr. Lutendo Nethwadzi and the Radiation Oncology Staff members both at RBMI and CMJAH for their assistance and patience during the course of my project.

Finally, I would like thank Charlotte Maxeke Johannesburg Academic Hospital (CMJAH) and Richards Bay Medical Institute (RBMI) for allowing me to use their hospital equipment and review the data necessary for this research project, without their go ahead, this research project could have not been possible to conduct.

TABLE OF CONTENTS

LIST OF FIGURES

Fig. 11. The PTW 10008 Unidos E electrometer (PTW Freiburg, Germany) used for the measurement of charge during CT,CBCT dosimetry and kilovoltage dosimetry on a radiotherapy simulator and Varian OBI is shown. (image copied from ref. 39)

Fig. 12. CT dose measurement setup at (A)-RBMI and (B)-CMJAH is shown, indicating the phantom, electrometer and the connecting cable from the ionization chamber to the electrometer.

Fig. 13. Scout scan acquired for the verification of the accuracy of phantom alignment is shown.

Fig. 14. CBCT dose measurement setup is shown. The center phantom was aligned to the isocenter of the linac at SAD of 100 cm.

Fig. 15. Alignment of the phantom using room lasers is shown.

Fig. 16. CBCT image acquired for the verification of the phantom alignment is shown. On the axial view, the actual isocenter of the system is indicated by the intersection of the green and red dotted lines, and the setup isocenter is indicated by the ion chamber located at the center position of the phantom. The alignment is indicated for axial, coronal and sagittal views.

Fig. 17. The set up for dosimetry on a kV planar Varian OBI is shown. The ion chamber was position at the SCD of 100 cm on top of white water phantom.

Fig. 18. The setup for measurements of radiographic dose on the radiotherapy simulator at CMJAH.

LIST OF TABLES

CHAPTER 1

1. INTRODUCTION

1.1 Brief history of X-rays and imaging

X-ray imaging began in late 1895 after X-rays where discovered by Dr. Wilhelm Conrad Roentgen[1], in Wurzburg, Germany. Roentgen was studying the effect of cathode rays on gases using a Crookes tube when he noticed that a piece of phosphorus material situated some distance away in his laboratory was glowing[1]. Fascinated by what he observed, he went on to study the mysterious rays in detail for weeks.

One of his significant observations was that the unknowns rays (X-rays) were able to penetrate some solids better that others (i.e. more penetration through soft tissue than bone)[1]. He announced the discovery at the Wurzburg Physical Medical Society in early 1896. In 1901, he was awarded the Nobel prize[1,2].

Within a few months after the announcement, X-ray tubes were set up to image the public for both medical and entertainment purposes, viewed at the time as a new form of photography. The medical importance of X-rays for diagnostic purposes was evident. Within a few months of their discovery, clinicians globally were using X-ray imaging to identify bone fractures[2].

A year later, the ability of X-rays to shrink tumors was discovered by a French physician, François-Victor Despeignes[3], marking the beginning of radiation therapy. During those years, the potential health hazards of X-ray exposure were unknown. The first dangerous side effects were reported by Dr. W Gage[4] late in 1896. He found that exposure to X-rays resulted in hair loss, reddened skin and skin lesions[4]. The dangers of exposure to ionizing radiation became better understood with time and they began to be used for only medical procedures rather than for entertainment purposes[2].

A cathode X-ray tube was later invented by William Coolidge[2] in 1913. The invention greatly improved the quality of X-ray images. Since then, advancements in X-ray imaging technology have been made, like the introduction of X-ray tomography in the 1940’s. The technique was achieved by rotating an X-ray tube around the human body, allowing a tomogram to be obtained. The imaging technology was further revolutionized with the introduction of computers in the 1970’s, enabling the X-ray images to be processed and reconstructed by a computer.

Two major advancements of the time were the invention of the Computed Tomography (CT) technique by Hounsfield and Cormack[5] in 1971 and the development of a Magnetic Resonance Imaging (MRI) technique by Raymond Damadia et al.[5] in 1976. Both were computerized tomographic techniques that could display cross sectional slices of a three dimensional object, but unlike the X-ray based CT, MRI does not require ionizing radiation.

Other significant imaging inventions of the time include medical ultrasound imaging (technique first used clinically in 70's and discovered in 1955)[5] and the gamma camera (in the 1950's by Hal Angerln)[6] marking the beginning of Nuclear Medicine. The first computerized 'tomoscanner' gamma camera was also developed in the 1970's. Imaging technology continues to advance to this day, driven by the need to achieve better image quality, improve imaging speed and to reduce imaging dose.

1.2 The need for imaging in radiotherapy

External beam radiotherapy is one of the most common treatment options for various types of cancers[7]. Radiotherapy is normally given over a number of fractions or daily sessions; this allows larger radiation doses to be delivered to the tumor and time for the repair of normal tissues, which reduces the side effects of treatment. The success of external beam radiotherapy primarily relies on how accurately the target or tumor within the patient is identified, how accurately the external radiation beams are directed towards the target and also the uniformity and conformity of the radiation dose to the target volume.

All of these tasks are significantly dependent on the Imaging technology being employed. Figure 1.1 indicates the three major steps during the modern radiotherapy process[7].

(1) Treatment planning

(2) Treatment delivery

(3) Post treatment assessment

All of these steps involve imaging. Images are required for three major reasons:

(1) Imaging for planning, in which the size, shape and depth of the target, and the surrounding normal tissue structures are identified using a CT scanner. Other imaging techniques like Positron Emission Tomography (PET) scanning or MRI scanning are at times used to provide additional information in order to more precisely localize the target.

(2) Imaging to check and verify the accuracy of patient's positioning and target localization before and during treatment.

(3) To assess the effectiveness of treatment by checking if the tumor has been eradicated or has shrunk.

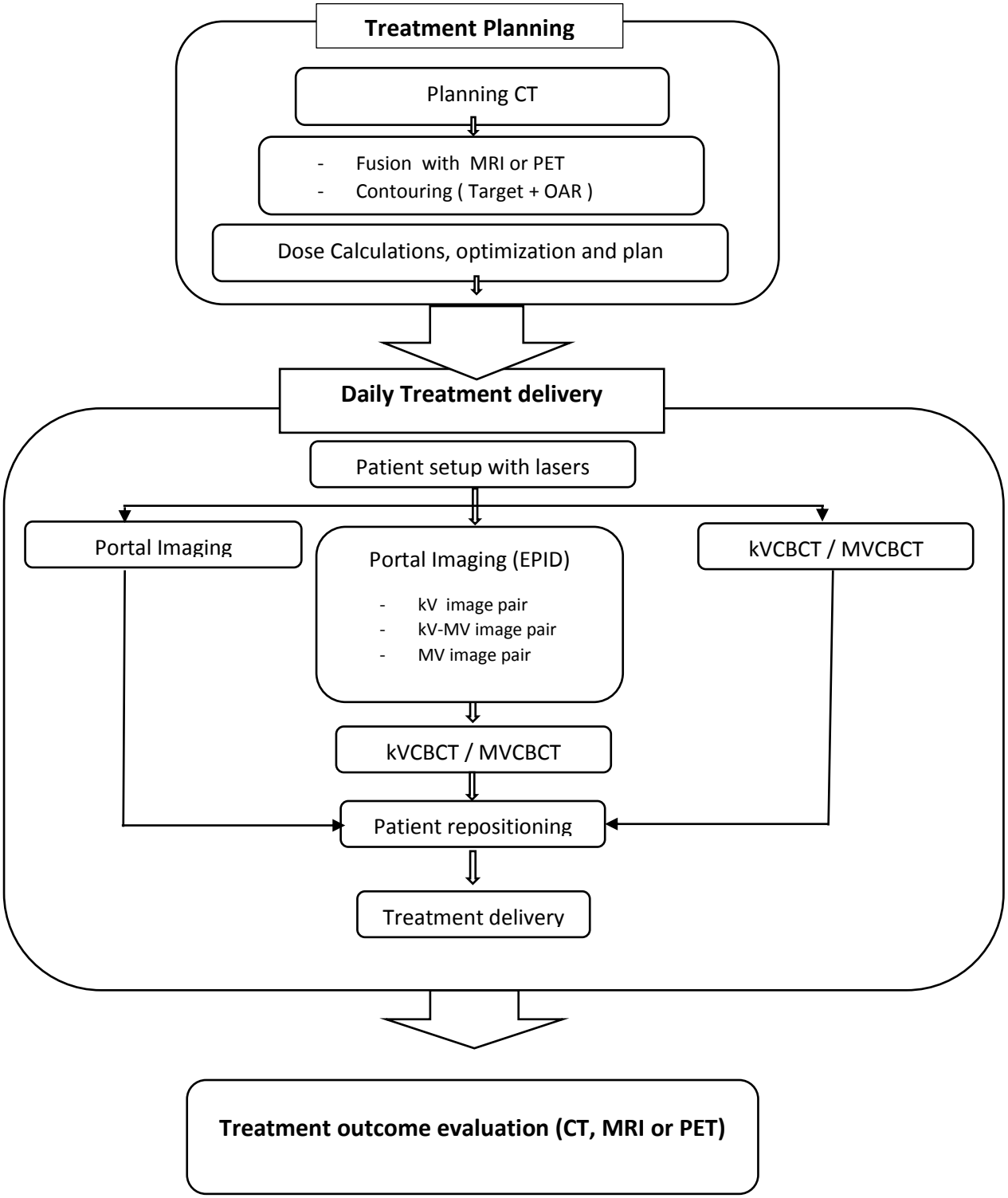

Fig. 1. Schematic presentation of the imaging process during Radiotherapy. kVCBCT/MVCBCT - Mega-Voltage/kilo-Voltage Cone Beam Computed Tomography; EPID - Electronic Portal Imaging Device; MRI - Magnetic Resonance Imaging; PET-Positron Emission Tomography; OAR - Organs At Risk

1.3 Concerns regarding the imaging dose

The imaging dose accumulated during the radiotherapy process has long been neglected partly because of its low magnitude in comparison to the high levels of therapeutic dose prescribed to treat patients. Recent advances in radiation treatment delivery such as 3D conformal radiation treatment (3DCRT) and intensity modulated radiation therapy (IMRT) enables the delivery of prescribed radiation doses to the target with great conformity and uniformity while minimizing the radiation dose to the surrounding normal structures, but this can only be achieved with accurate target localization. The need to achieve this objective has led to advances in imaging technology, and as a result the increased imaging has led to increased imaging dose. The primary concern is the induction of secondary cancers, due to exposure of normal tissue volumes extending beyond the volume of interest during imaging[8].

The reported radiation exposure from all medical procedures in the National Council on Radiation Protection and Measurements (NCRP) report No 160, of March 2006, was 3 mSv, an increase of nearly 500% compared to the reported exposure of 0.34 mSv in the NCRP report 93, of the 80's[9,10].

The comparison of medical exposures to patients reported in NCRP reports No 93 and 160 is listed in Table 1. Amongst different imaging modalities listed, CT was the largest contributor to the overall increase in medical exposures. The technological advancement made in the past two decades has made it easier for CT technology to be applied in many clinical applications.

According to the United Nations Scientific Committee on the Effects of Atomic Radiation (UNSCEAR) 2008 report, the CT accounts to about 7 % of all X-ray examinations globally, contributing approximately 43 % to the total annual collective dose[11,12], with the average effective dose from all radiological procedures worldwide increasing from 0.38 mSv to 0.62 mSv in the period of 1988-2007[12].

MODALITY	NCRP REPORT NO 93 (EARLY 80'S)	NCRP REPORT NO 160 (MARCH 2006)
CT	3%	49%
Nuclear Medicine	26%	26%
Conventional Fluoroscopy and Radiography	68%	11%
Interventioanl Fluoroscopy	3%	14%

Table 1. Comparison of medical exposure of patients in USA between 1980 and 2006 from various medical procedures, indicating a very high increase due from CT procedures[9,10].

1.4 Imaging Scenarios for image guided radiation therapy (IGRT)

1.4.1 CT-Imaging for planning

CT imaging is the first step in modern radiotherapy planning process whereby images are acquired in the treatment position for target definition. The ability of a CT to display three dimensional internal structures with good contrast and to directly measure electron densities makes it an ideal imaging modality specifically for the purpose of organ delineation and dose computation[13].

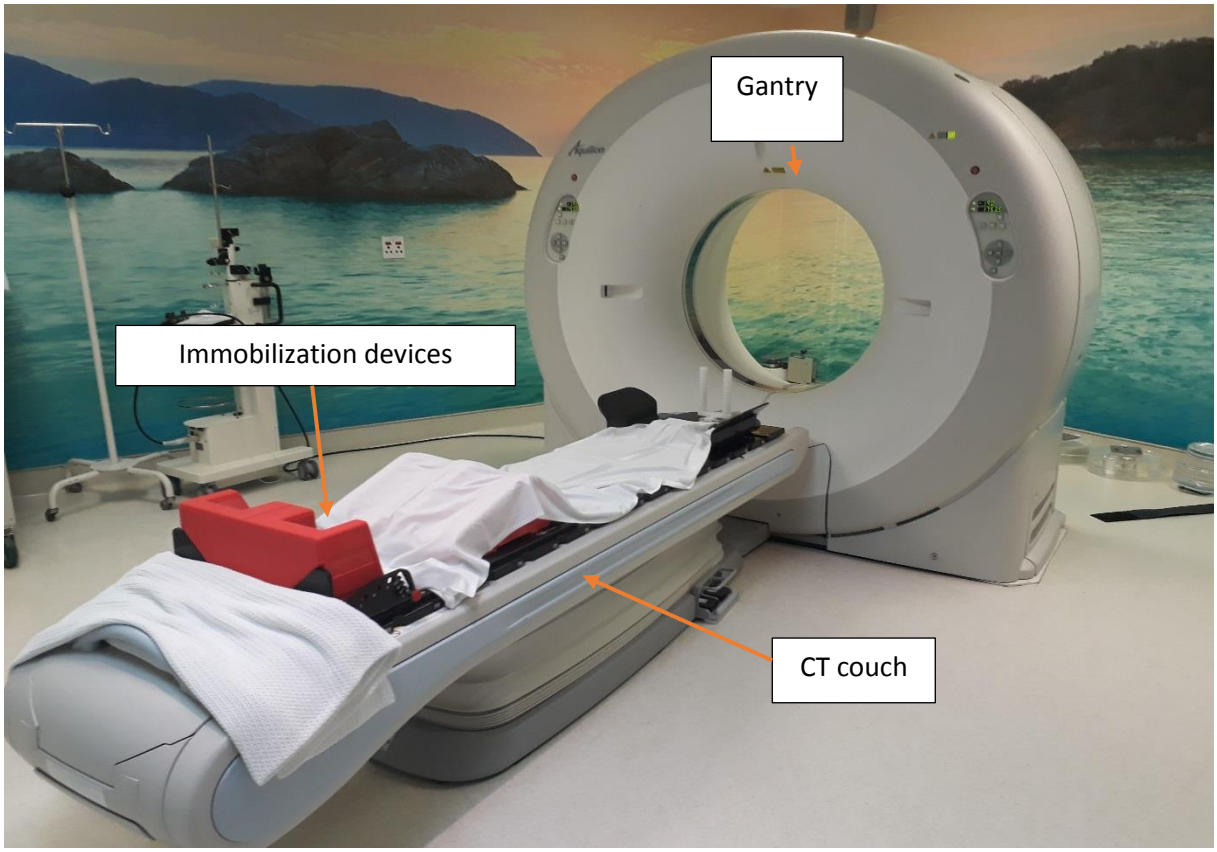

Fig. 2. A typical CT Simulator used in Radiation Therapy is shown.

During imaging for planning, a patient is placed on the couch with immobilization devices to minimize the patient's movement during scanning and to ensure reproducibility of the position for treatment. The patient is then setup with the region of interest to be scanned aligned to the CT lasers, which indicate the centre of the CT gantry. Once complete, two lateral and one anterior radio-opaque balls are placed on the skin surface in alignment with the isocenter of the horizontal and vertical plane of the lasers. The three balls provide external markers that indicate a known reference point that is used in the treatment planning system and the actual treatment machine (clinical linear accelerator)[13]. Once the scan has been completed, the patient is marked with permanent tattoos on the skin where the balls were placed.

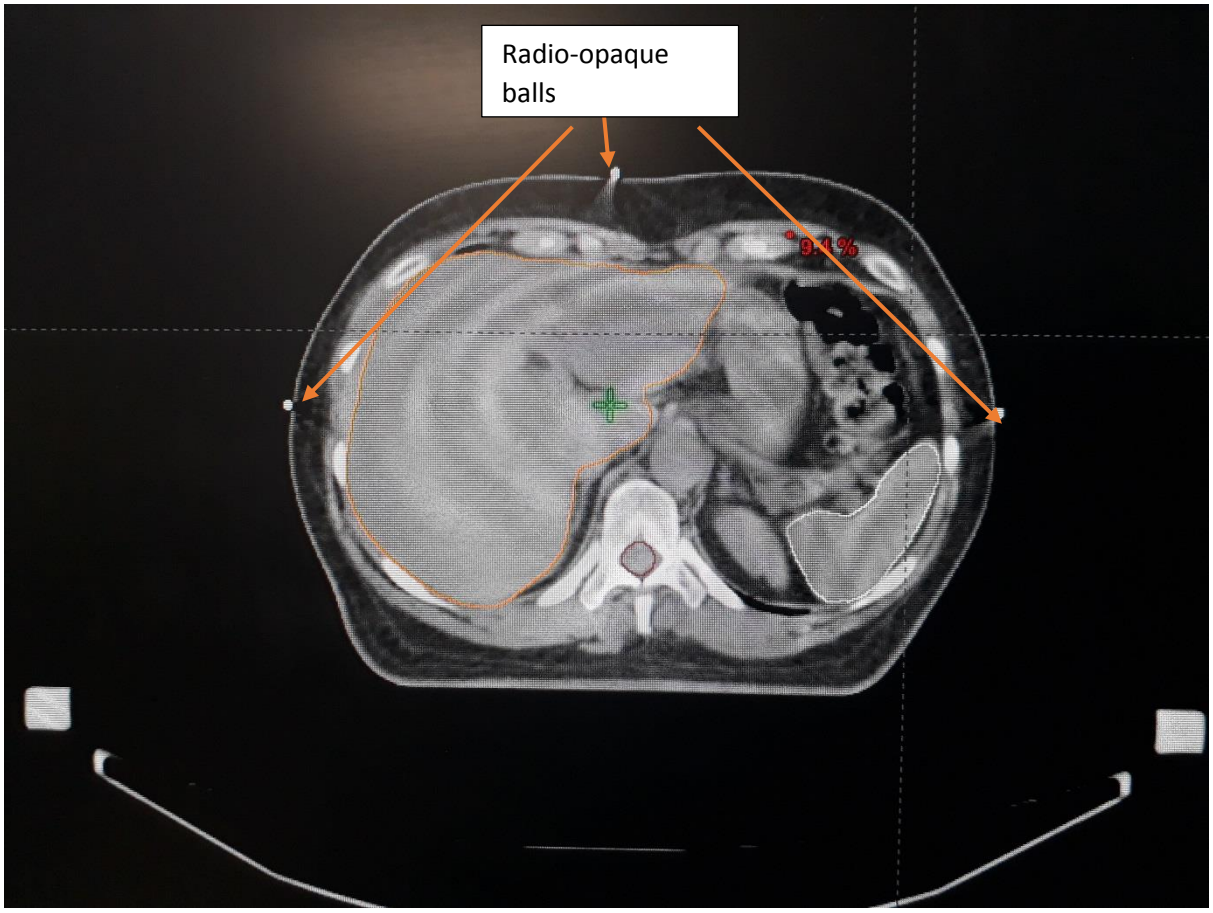

Fig. 3. Axial CT slice with three opaque balls placed on the patient's skin.

1.4.2 Treatment simulation

Patient simulation is a process that involves:

- Determination of beam geometry, tumor volumes, organs at risk and the treatment position of the patient
- Generation of simulation radiographs or Digitally reconstructed radiographs (DRRs)

Historically, planar simulator radiographs were obtained from a conventional radiotherapy simulator, which is a radiography/fluoroscopy system with the ability to mimic most of the geometries of isocentric treatment machines. A typical conventional simulator is shown in Fig. 5.

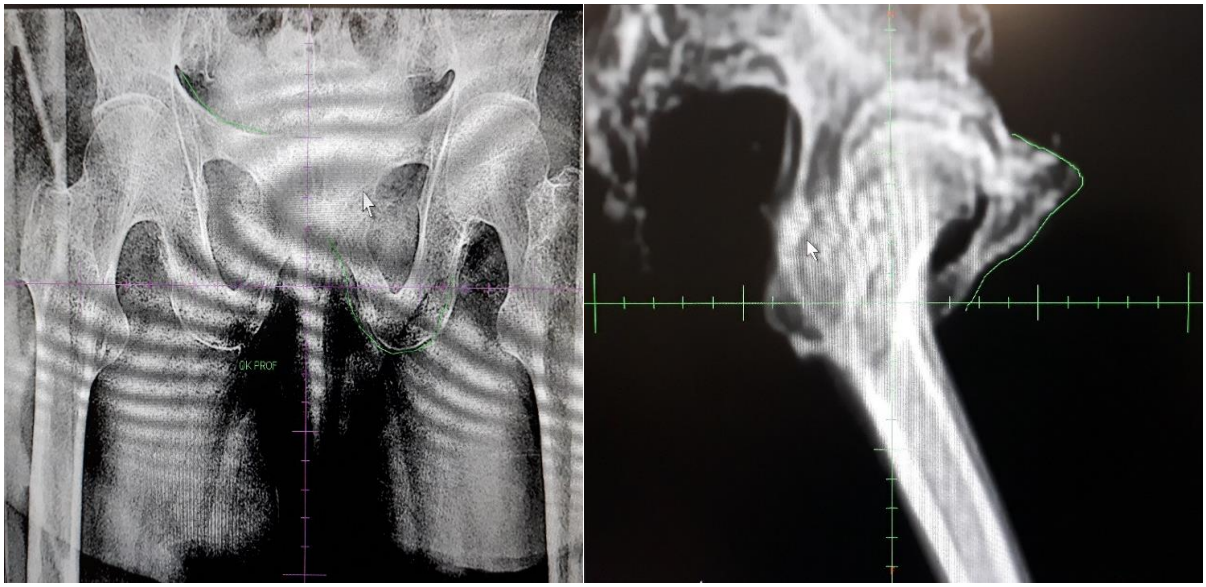

Fig. (4). A Set of digitally reconstructed radiographs (DRR's), anterior-posterior and lateral views respectively, reconstructed from a planning CT at RBMI.

In virtual simulation, simulation images and DRRs are generated directly from the planning CT information.

Fig. 5. A typical radiotherapy treatment simulator is shown. A Simulator can produce treatment geometries that can be obtained on a treatment machine. (Image copied from ref. 14)

1.4.3 Setup verification

The precise delivery of the planned radiation treatment is dependent on the accuracy of patient treatment position. This is achieved by comparing the simulator radiographs or DRRs with in-room images acquired before patient treatment. Traditionally portal images were generated on films (Port films)[13], but with recent advances in imaging technology, there exists a variety

of imaging modalities such as EPID- based MV planar imaging, kV planar imaging, and kV and MV cone beam computed tomography (CBCT)[15]. CBCT enables direct comparison of CBCT images with the planning CT images for internal soft tissue target alignment.

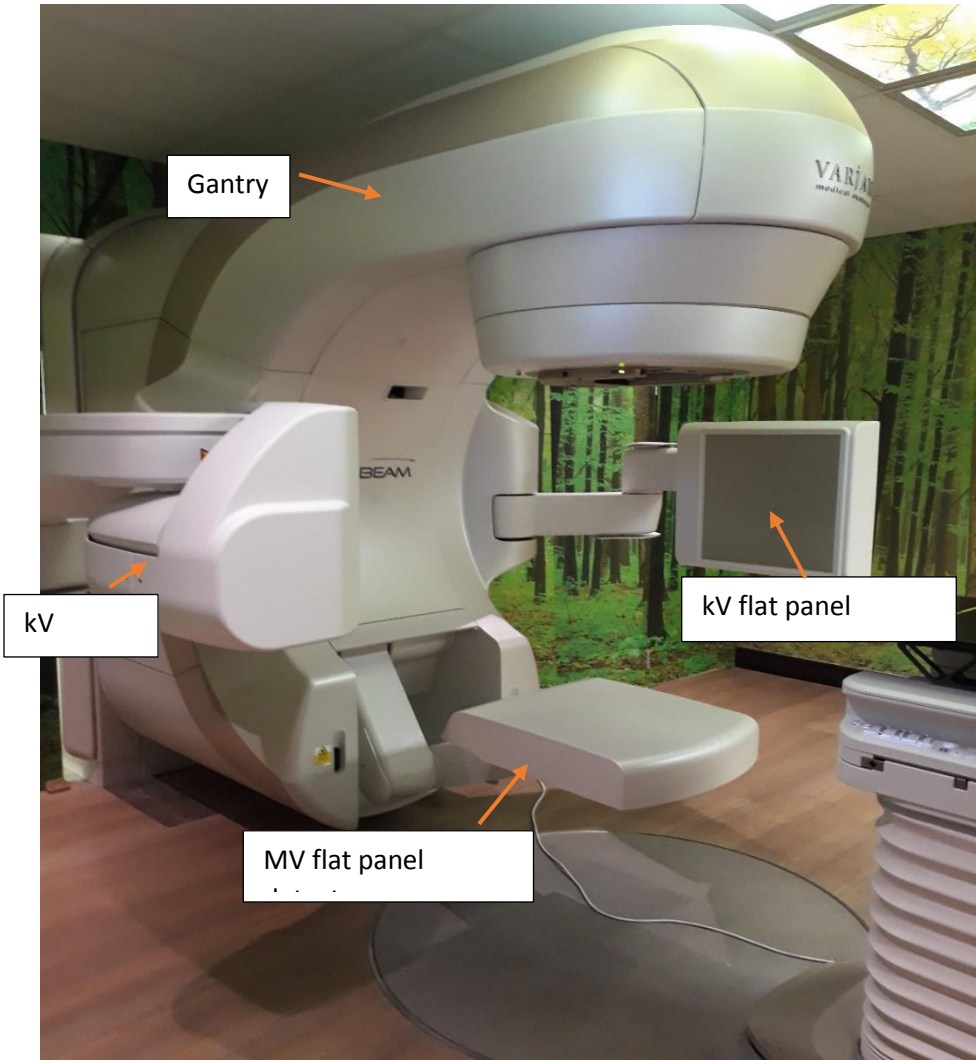

Fig. 6. A modern Medical Linear Accelerator with kVCBCT, planar kV and MV imaging capabilities is shown.

Some institutions employ imaging modalities like in-room CT. The in-room CT provides an added advantage of producing the same image quality as the planning CT and also enables soft tissue target alignment[13,15].

1.5 Research objectives

A lot of research has been devoted to the assessment of the X-ray imaging dose from different imaging techniques due to an increase in the utilization of X-ray imaging. CBCT dose has been assessed by a variety of researchers[16-22]. Extensive research has been conducted in dosimetry in diagnostic radiology and a number of guidelines and codes of practice exist for measurement of dose in CT and other diagnostic X-ray imaging modalities[23-28].

Though measurement and evaluation methods exist for assessment of imaging dose from a variety of imaging modalities, little effort has been devoted to the measurement and evaluation of the total imaging dose from all imaging modalities used for patient imaging during the radiotherapy process.

The American Association of Physicist in Medicine (AAPM) task group (TG) 75[15], issued a report on management of imaging dose during IGRT, with guidelines outlining how to evaluate and measure the imaging dose. This Study aims to adopt the same methodologies used in the report to measure, evaluate and compare the total imaging dose and the resulting effective dose received by patients during typical radiotherapy processes from different imaging modalities at 2 different centres.

CHAPTER 2

2. BACKGROUND

2.1 Computed Tomography

During the early days of CT, it became evident that the dose concepts applicable to projection radiography could not be used to CT for a variety of reasons[29],

- The CT dose distribution is different from that of a conventional radiogram, in the sense that in CT, the patient is homogeneously irradiated along the scanning direction.
- The CT radiation beams are narrow shaped fan-beams, this implies that there is a significant amount of energy deposition outside the nominal beam width.

2.1.1 The CT dose index

The first dose descriptor and a standard for determination of radiation dose in a fan beam CT was the multiple scan average dose (MSAD)[29]. The MSAD is defined as the dose from multiple scan examinations, averaged over one scan interval along the longitudinal scan axis[29]. It is typically presented in dose unit of mGy.

The process of determining the MSAD was intensive and time consuming as it required the acquisition of multiple axial CT scans and additional time to allow the X-ray tube to cool down in between measurements. This led to the development of computed tomography dose index (CTDI). The CTDI concept was first introduced by Shope et al.[26] in 1981, defined as the integral of the single scan radiation dose profile along the scan longitudinal axis, normalized to the thickness of the imaged section[26]. They proved that CTDI can be used to estimate the MSAD by applying the correction for scan spacing or pitch, allowing all of the scatter tails from radiation dose profiles to be included in the CTDI measurement. The CTDI provided a simple and convenient method in the determination of CT dose and is presently the primary concept in CT dose measurement. The mathematical description of a CTDI[23-28], is shown in Equation 1, where

$$\mathrm{CTDI} = \frac{1}{\mathrm{NT}} \int_{-\infty}^{\infty} \mathrm{D(z)d(z)} \qquad (1)$$

- D(z) is the dose profile along the scan direction
- N is the number of tomographic slices acquired
- T is the slice width

The CTDI is typically measured using a 100 mm long ionization chamber and standardized phantoms that consist of two acrylic cylinders that are 15 cm in length, and 16 cm and 32 cm in diameter representing the head and body sections of an adult respectively[28]. The CT phantoms and ionization chamber are shown in Fig. 7 and Fig. 8 respectively. The $CTDI_{100}$ represents the MSAD dose at the center of a 100 mm scan[29]. For scan lengths greater than 100 mm, the $CTDI_{100}$ underestimates the MSAD because of the exclusion of scatter tails beyond 100 mm range. The mathematical description of $CTDI_{100}$[28,29], indicating the standardized scan range of 100 mm is shown in Equation 2. The CTDI is calculated using Equation 3.

$$\mathrm{CTDI_{100}} = \frac{1}{\mathrm{NT}} \int_{-50\mathrm{mm}}^{50\mathrm{mm}} \mathrm{D(z)d(z)} \tag{2}$$

$$CTDI = \frac{1}{NT} \times \bar{M} \times N_{PklQ0} \times K_Q \times K_{TP} \tag{3}$$

Where,

- K_{TP} is the air density correction factor
- $\mathrm{N_{PklQ0}}$ is the ionization chamber calibration factor
- $\bar{\mathrm{M}}$ is the mean dosimeter reading
- $\mathrm{K_Q}$ is the beam quality correction factor.

2.1.2 Weighted CTDI ($CTDI_w$)

In general, the radiation dose decreases with depth as it penetrates matter through a variety of interactions[30]. As a result, the dose is higher at the surface than in the center[28,29]. In an attempt to address this variation, the weighted CTDI ($CTDI_w$) is used in order to determine the average dose across the FOV. The $CTDI_w$ is mathematically described in Equation 4, where

$$\mathrm{CTDI_w} = \frac{1}{3}\mathrm{CTDI_{100,center}} + \frac{2}{3}\mathrm{CTDI_{100,periphery}} \quad (\mathrm{mGy}) \tag{4}$$

- $\mathrm{CTDI_{100,center}}$ is the $CTDI_{100}$ representing the center dose in a phantom
- $\mathrm{CTDI_{100,periphery}}$ is the $CTDI_{100}$ representing the surface dose in phantom

2.1.3 Volume CT dose index ($CTDI_{vol}$)

To accommodate different scan protocols during CT examinations and gaps or overlap of dose profiles[29], $CTDI_{vol}$ was used. It is defined as the ratio of the $CTDI_w$ to the scan pitch. It represents the dose from a specific scan protocol. Shown in Equation 5 and 6 are mathematical descriptions of $CTDI_{vol}$ and pitch respectively[23-29]. Theoretically, for a pitch factor of 1, $CTDI_w$ is equivalent to $CTDI_{vol}$.

$$\mathrm{CTDI_{VOL}} = \frac{\mathrm{CTDI_W}}{\mathrm{pitch}} \quad (\mathrm{mGy}) \tag{5}$$

$$\mathrm{pitch} = \frac{\mathrm{I}}{\mathrm{NT}} \tag{6}$$

2.1.4 Dose length product (DLP)

Patient CT examinations often exceed 100 mm scan length, which is used during $CTDI_w$ measurements[24,28,29]. In an attempt to accurately estimate the dose from the entire CT examination, the $CTDI_{vol}$ is integrated along the actual scan length of the CT examination to compute the DLP. The mathematical description of the DLP defined by Equation 7.

$$DLP = CTDI_{VOL} \times \text{scan length} \quad (mGy \cdot cm) \tag{7}$$

2.2 Dosimetry in kV radiography

This report follows the methodology of the International Atomic Energy Agency (IAEA) Technical Report Series (TRS) number 457[28] to estimate the patient dose by measurement of entrance surface air kerma (ESAK). According to the IAEA TRS 457, patient dose in general radiography is determined by three principal quantities, incident air kerma (K_i), ESAK and air kerma area product (KAP) [28]. Kinetic Energy Released in the Medium per unit mass (KERMA), represents the amount of energy transferred from radiation to matter. Though different from the absorbed dose, which represents the amount of energy deposited in matter per unit mass, the distinction between the two is negligible for low X-ray energies, hence in some literature ESAK is also referred to as entrance surface dose (ESD).

2.2.1 Air kerma (K_a), K_i, ESAK and the air KAP

ESAK is defined as the air kerma on the X-ray beam central axis at the patient or phantom surface[28]. It is typically measured using a 20 cm thick water or PMMA phantom with a plane parallel plate ionization chamber[28]. Similarly to ESAK, K_i is defined as the air kerma measured free in air at the position of the patient or phantom surface[28], excluding backscatter. Air kerma from the X-ray machine, at the source to chamber distance (SCD) d, for a given exposure settings (kVp and mAs) is calculated using Equation 8.

$$K(d) = \bar{M} \times N_{K,Q0} \times K_Q \times K_{TP} \tag{8}$$

Where,

- M is the mean dosimeter reading collected at SCD.
- $N_{K,Qo}$ is the calibration factor for the ionization chamber
- K_Q is the beam quality correction factor
- K_{TP} is the air density correction factor.

The X-ray unit Output Y (d), is calculated as the ratio of the air kerma to the tube loading P_{It}[28], as shown in Equation 9.

$$Y(d) = K(d)/P_{It} \quad (9)$$

K_i is calculated using the relation shown in Equation 10, and the inverse square law is applied to derive the air kerma incident on the patient

$$K_i = Y(d) \times P_{It} \times \left(\frac{d}{D-t}\right)^2 \quad (10)$$

Where,

- d is source to chamber distance
- D is the source to table distance
- t is the thickness of the patient or phantom

The relationship between ESAK and K_i is described in Equation 11.

$$ESAK = K_i \times \text{Backscatter factor (BSF)} \quad (11)$$

When ESAK measurements are made directly on the 20 cm thick Acrylic at a source to chamber distance of 100 cm, the ESAK is calculated using Equation 12.

$$\mathrm{ESAK} = \bar{M} \times N_{K,Q} \times K_Q \times K_{TP} \times \frac{BSF_W}{BSF_{acrylic}} \quad (12)$$

By definition, KAP is air kerma in a plane, integrated over the area of interest. It represents the total amount of radiation incident on the surface area of the patient or phantom. KAP is described in Equation 13, it is the product of the entrance surface dose and the exposed area.

$$\mathrm{KAP} = \mathrm{ESAK} \times \mathrm{area} \quad (13)$$

2.3 6 MV and Cobalt-60 portal dose

Radiotherapy linear accelerators (linacs) are typically calibrated to deliver a dose rate of 1cGy per monitor unit (MU) at a reference depth t_o, fixed source to calibration distance (SCD) and in a reference field size of 10 × 10 cm[7]. For fixed isocentric treatment techniques, the monitor units (MU) required to deliver a dose D to the isocenter at depth d is given by Equation 14[7]. For linacs that have been calibrated isocentrically, SCD is equal to the source to axis distance (SAD), which is typically 100 cm and SAD factor is 1.

$$\mathrm{MU} = \frac{D}{K \times TMR(d, r_d) \times S_c \times S_p \times \text{SAD factor}} \quad (14)$$

Where,

- K = 1cGy per MU
- S_c is the collimator scatter factor
- S_p is the phantom scatter factor
- TMR is the tissue maximum ratio

For a given number of monitor units delivered during imaging, the dose to the isocentre is similarly defined by Equation 15.

$$D = \mathrm{MU} \times \text{total Output Factor (OF)} \quad (\mathrm{cGy}) \quad (15)$$

Where the total OF (cGy/MU) is the product of the factors in the denominator in Equation 14. The dose from a cobalt-60 therapy unit is described by Equation 16.

$$D(\mathrm{cGy}) = \frac{\text{Time(min) x Dose rate(cGy /min)}}{\text{Output factor}} \quad (16)$$

2.4 Estimation of the effective dose

The imaging dose during radiotherapy is accumulated from a variety of imaging techniques. As a result the dose distribution resulting from each imaging scenario is different. Because of the difference, the direct addition of dose in such instances is inappropriate and misleading because of the variation of the resulting biological effects associated with each imaging scenario[15]. AAPM TG-75[15] recommends that the doses be converted to effective dose, which is a quantity that is representative of the radiobiological effect, prior to addition or comparison. The concept of effective dose was first introduced in 1975 by Wolfgang Jacobi [31], defined as "the mean absorbed dose from a uniform whole-body irradiation that results in the same total radiation detriment as from the non-uniform, partial-body irradiation". The Effective dose cannot be measured directly, but is calculated as the sum of the product of equivalent dose values to the various exposed organs and their organ weighting factors to obtain an equivalent whole body dose. Various researchers have published factors that allow for the estimation of the effective dose without having to measure organ specific doses[15,23,32-35]. Using such conversion factors, the effective dose can be calculated using Equation 17[15].

$$\mathrm{E\ (mSv)} = \mathrm{D(mGy)} \times \mathrm{F(mSv\ per\ mGy)} \tag{17}$$

Where,

- E is the effective dose (mSv)
- D is the absorbed dose (mGy)
- F is the semi empirical organ weighting conversion factor(mSv per mGy)

CHAPTER 3

3. MATERIALS AND METHODS

3.1 Imaging Modalities

This study was conducted at the Charlotte Maxeke Johannesburg Academic Hospital (CMJAH) and Richards Bay Medical Institute (RBMI). Dose measurements at CMJAH were carried out on a GE High speed NXi CT scanner and a Toshiba LX40 radiotherapy simulator. The MV portal dose on a Siemens Primus linac and a Cobalt radiotherapy unit was calculated using the tabulated clinical beam data based on the electronic records of the portal imaging carried out. Dose measurements at RBMI were carried out on a Toshiba Aquilion LB CT Scanner, and the Varian On Board Imager (OBI) for kV planar imaging and kV cone beam CT.

3.2 Dosimetry equipment

3.2.1 CT and CBCT Phantom

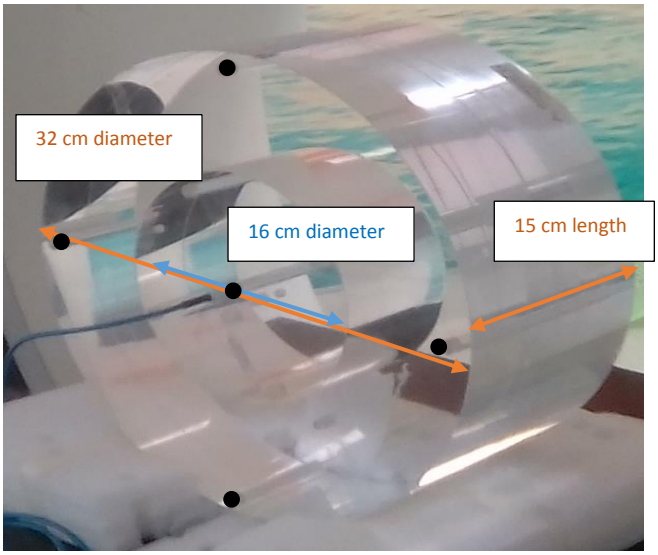

Fig 7. The two in one head and body acrylic phantom (PTW Freiburg, Germany) used for CT and kVCBCT dosimetry at RBMI and CT dosimetry at CMJAH is shown. The 16 cm diameter cylinder represents the head section and the 32 cm diameter represents the body section. Both cylinders are 15 cm in length. The holes for the insertion of the ion chamber for measurements of the center and peripheral CTDI are indicated by black dots. The phantoms have been standardized by the FDA[36].

3.2.2 CT Ionization chamber

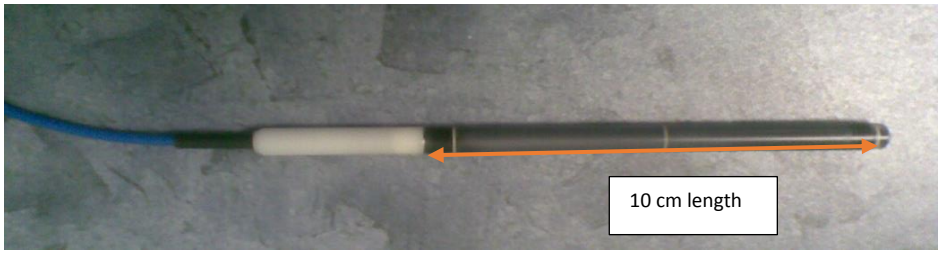

Fig. 8. The CT PTW 30009 pencil ionization chamber (PTW Freiburg, Germany) with sensitive length of 10 cm is shown. The ion chamber calibration factor used during measurements is traceable to Bureau International des Poids et Mesures (BIPM) [37]. BIPM is the international laboratory with the primary role of development and maintenance of standards.

3.2.3 Backscatter phantoms for kV dosimetry

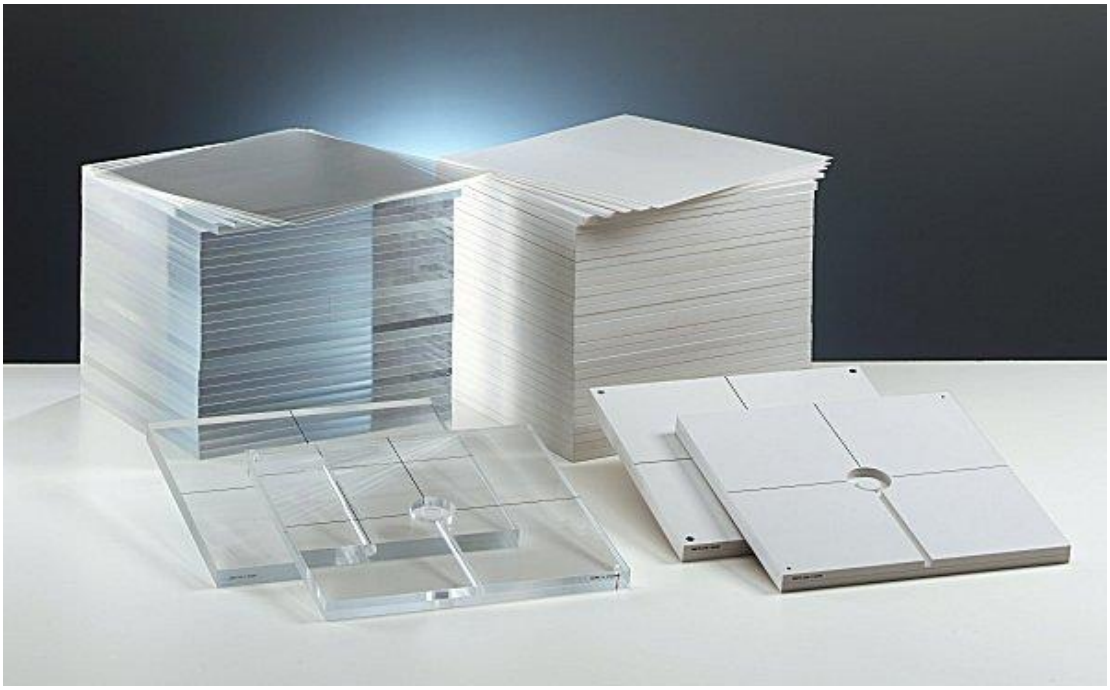

Fig. 9. The PTW acrylic and water-equivalent RW3 (PTW Freiburg, Germany) slabs are shown. To provide for backscatter, the slabs are placed below the ion chamber. The size of each slab is 30 × 30 cm^2, with varying thickness, typically of 1 mm, 2 mm, 5 mm and 10 mm.(image copied from ref. 38)

3.2.4 Parallel plate ionization chamber used for kV dosimetry

Fig. 10. The PTW TM77334 parallel plate ionization chamber(PTW Freiburg, Germany) is shown. The given calibration factor for the ion chamber was traceable to BIPM.

3.2.5 Electrometer

Fig. 11. The PTW 10008 Unidos E electrometer (PTW Freiburg, Germany) used for the measurement of charge during CT,CBCT dosimetry and kilovoltage dosimetry on a radiotherapy simulator and Varian OBI is shown. (image copied from ref. 39)

3.3 Methodology

3.3.1 CT dosimetry at CMJAH and RBMI

The CT dosimetry at CMJAH and RBMI was carried out using the body and head CT phantoms with a 100 mm PTW 30009 pencil ionization chamber connected to a PTW 10008 Unidos E electrometer. The center of the phantom was aligned to the isocenter of the CT scanner by aligning the phantom etched crosshairs to the CT lasers. The measurement setup is shown in Fig. 12. Once the setup was completed, a scout scan was acquired to check the accuracy of the phantom alignment and to ensure that the intended scan length of 100 mm was within the sensitive volume of the ionization chamber. The scout scan is shown in Fig. 13. The slice thickness of 5 mm, and the scan range of 100 mm was selected for both body and head measurements.

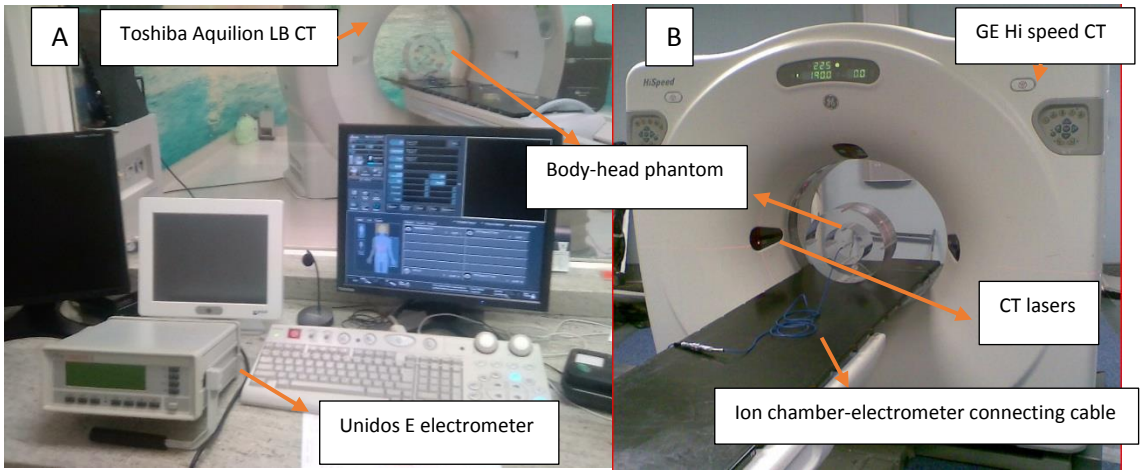

Fig. 12. CT dose measurement setup at (A)-RBMI and (B)-CMJAH is shown, indicating the phantom, electrometer and the connecting cable from the ion chamber to the electrometer.

The ambient room temperature and pressure were measured prior to measurements to enable the correction of the ion chamber response in the user's measurement environment to that of calibration. Three electrometer reading were collected in each of the five measurement holes in phantom. For each hole measurement, the remaining holes were filled with acrylic dummy plugs to ensure that the phantom was uniform. The $CTDI_{100}$ for both the center and peripheral positions of the ionization chamber was calculated using Equation 3. The acquisition parameters set during measurements are shown in table 2.

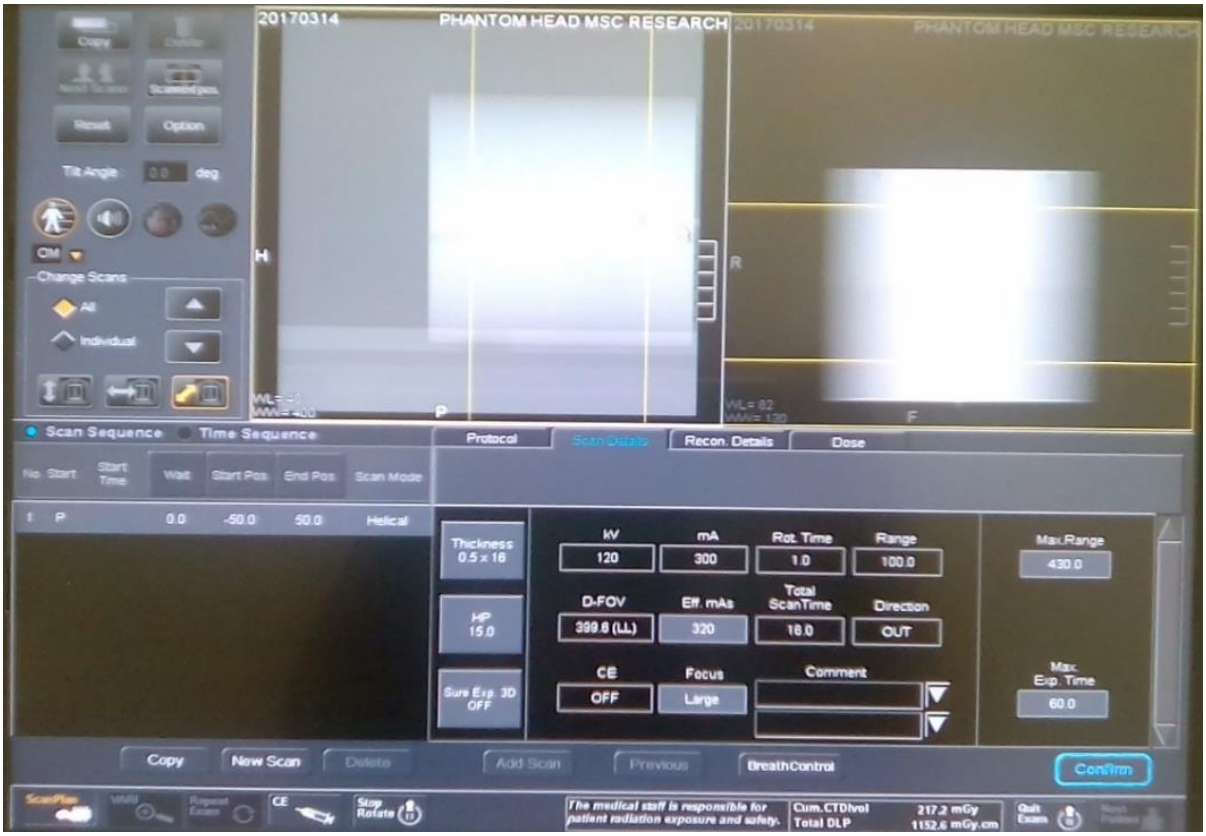

Fig. 13. Scout scan acquired for the verification of the accuracy of phantom alignment is shown.

Acquisition parameters	CMJAH		RBMI	
	HEAD	BODY	HEAD	BODY
Tube voltage (kVp)	120	120	120	120
Tube current (mA)	175	350	300	350
Scan time (s)	20	20	15.8	6.7
Scan range (mm)	100	100	100	100
Tube rotational time (s)	-	-	1	0.755
Slice thickness (mm)	5	5	5	5
Scan type	Axial	Axial	Helical	Helical

Table 2. CT scan acquisition parameters for the measurement of CT dose index using the head and body phantom at CMJAH and RBMI.

3.3.2 kVCBCT dosimetry on the Varian OBI

Measurements were carried out using the head and body CT phantom, with the 100 mm ionization chamber connected to the electrometer

The center of the cylindrical phantom was positioned at the isocenter of the linac, by aligning the etched crosshairs on the phantom with the room lasers. The collimation of the Y blades on the kV source were set to -50 mm and 50 mm such that the total collimation in the longitudinal direction was 10 cm at the isocenter to conform to the sensitive length of the ionization chamber in the center position of the phantom. The accuracy of the setup was checked by acquiring a CBCT, shown in Fig. 12. Similarly to the CT measurements, three electrometer readings were collected in each of the five holes the ion chamber was inserted. The set up for measurements is shown in Fig. 13 and Fig. 14. Measurements were taken at the kV source to axis distance (SAD) of 100 cm, with the kV image detector at a distance of 50 cm from the isocentre.

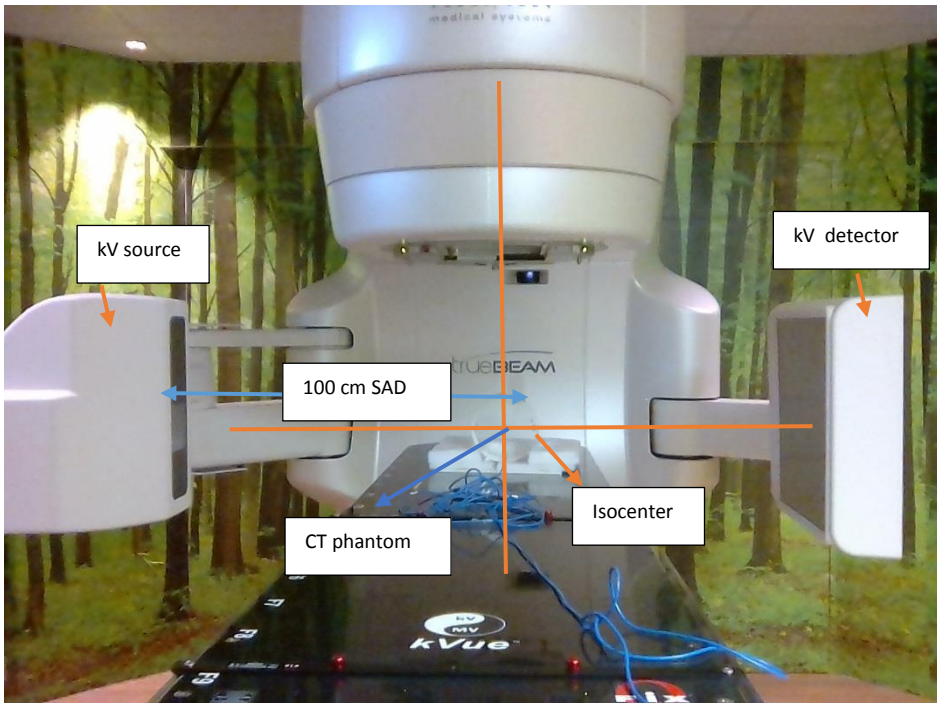

Fig. 14. CBCT dose measurement setup is shown. The center phantom was aligned to the isocenter of the linac at SAD of 100 cm.

Fig. 15. Alignment of the phantom using room lasers is shown.

Fig. 16. CBCT image acquired for the verification of the phantom alignment is shown. On the axial view, the actual isocenter of the system is indicated by the intersection of the green and red dotted lines, and the setup isocenter is indicated by the ion chamber located at the center position of the phantom. The alignment is indicated for axial, coronal and sagittal views.

The measurements were carried out using the Varian OBI imaging protocol exposure settings for imaging of the head and pelvic section. The exposure settings for head and pelvis imaging protocol are indicated in below table.

Image acquisition settings	Head protocol	Pelvis protocol
X-ray voltage (kVp)	100	125
X-ray current(mA)	20	80
X-ray millisecond(ms)	20	13
Fan type	Half	Full
Blade Y1(cm)	-5	-5
Blade Y2(cm)	5	5
Blade X1(cm)	-23.9	-13.2
Blade X2(cm)	2.6	13.2
Scan start(deg)	175.5	175.5
Scan stop (deg)	184.5	184.5
Total mAs	264	1056
Number of projections	656	654
Trajectory	full	full

Table 3. CBCT Scan acquisition parameters for the measurements of CBCT dose are indicated. The Y blades were set to the length of 10 cm at SAD of 100 cm to conform to the length of the ion chamber at the center position of the phantom

3.3.3 kV radiography dosimetry on the Varian OBI

Measurements were carried out using the PTW TM77334 parallel plate ionization chamber connected to the electrometer, and placed on a water equivalent polystyrene slab phantom to provide backscatter. The source to chamber distance was 100 cm. The measurement field size was set to 20 × 20 cm^2. A fixed field size of 20 × 20 cm^2 was chosen to estimate patient doses as the actual field sizes used during the exam could not be traced from the information management system. The setup is shown in figure 14. Dose Measurements were made using the imaging protocol exposure parameters for head and pelvis imaging. The Varian OBI half value layer specification (i.e. 70 kVp > 1.5 mm Al and 100 kVp > 2.7 mm Al) were assumed during measurements. The exposure parameters for imaging of the head and pelvis for both anterior-posterior (AP) and lateral projection are indicated in table 4.

HEAD PROTOCOL

Projection	mA	mAs	kV
AP	72.0	3.6	85
LAT	48.0	2.4	65

PELVIS AP PROTOCOL

Size	mA	mAs	kV
Small	48.0	2.4	75
Medium	64.0	3.2	75
Large	80.0	4.0	75
Extra large	96.0	4.8	75

PELVIS LATERAL PROTOCOL

Size	mA	mAs	kV
Small	95.0	9.6	120
Medium	95.0	9.6	120
Large	93.0	20.0	120
Extra large	93.0	20.0	120

Table 4. The exposure parameters for the imaging of the head and pelvis are indicated, the same setting were used during measurements in a phantom.

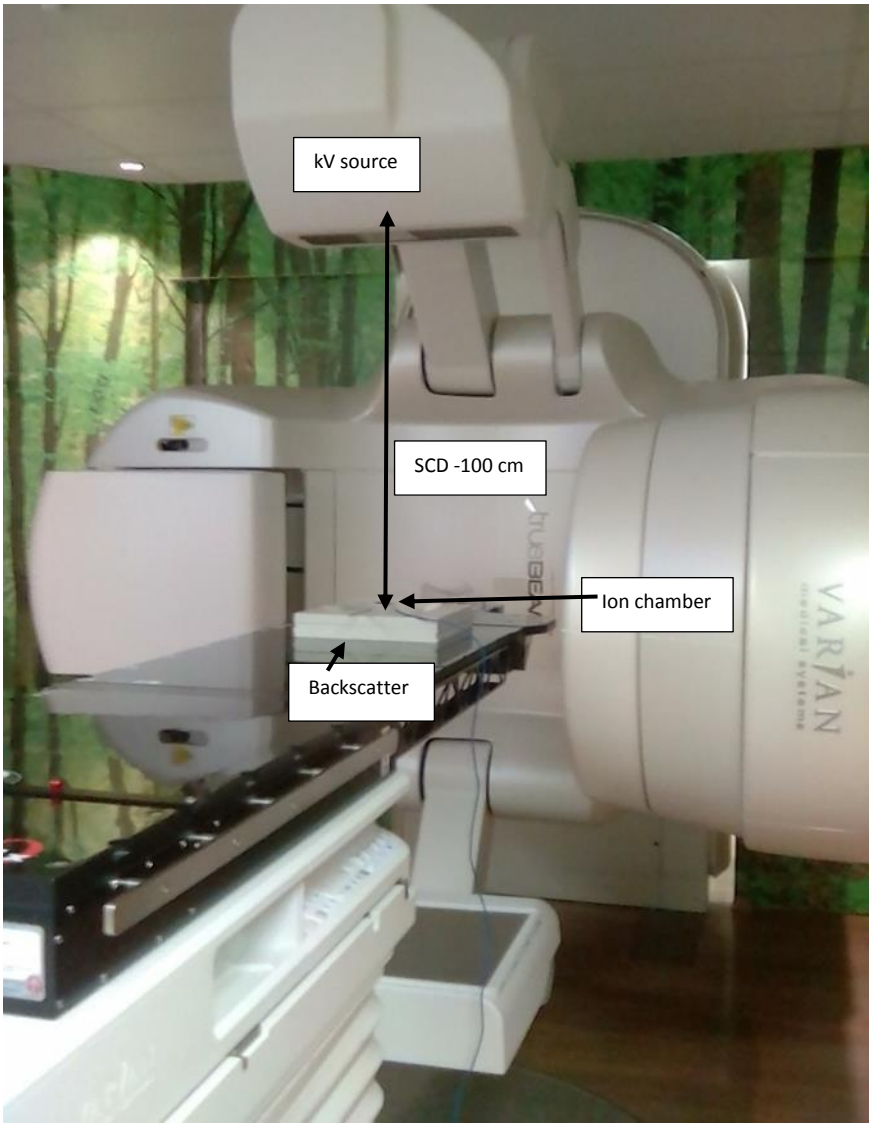

Figure 17. The set up for dosimetry on a kV planar Varian OBI is shown. The ion chamber was position at the SCD of 100 cm on top of white water phantom.

3.3.4 kV radiography dosimetry on the Toshiba simulator

Measurements were carried out using a PTW TM77334 parallel plate ion chamber connected to the PTW-Freiburg Unidos electrometer. The ion chamber was placed on top of a 30 × 30 × 30 cm^3 acrylic phantom to provide backscatter. The field size was set to 20 × 20 cm^2 at the source to chamber distance (SCD) of 100 cm. The ion chamber was positioned such that its entrance window center was on the central axis of the X-ray beam. Three electrometer readings were collected per measurement exposure settings. The room temperature and pressure was measured using the calibrated barometer and thermometer prior to measurements.

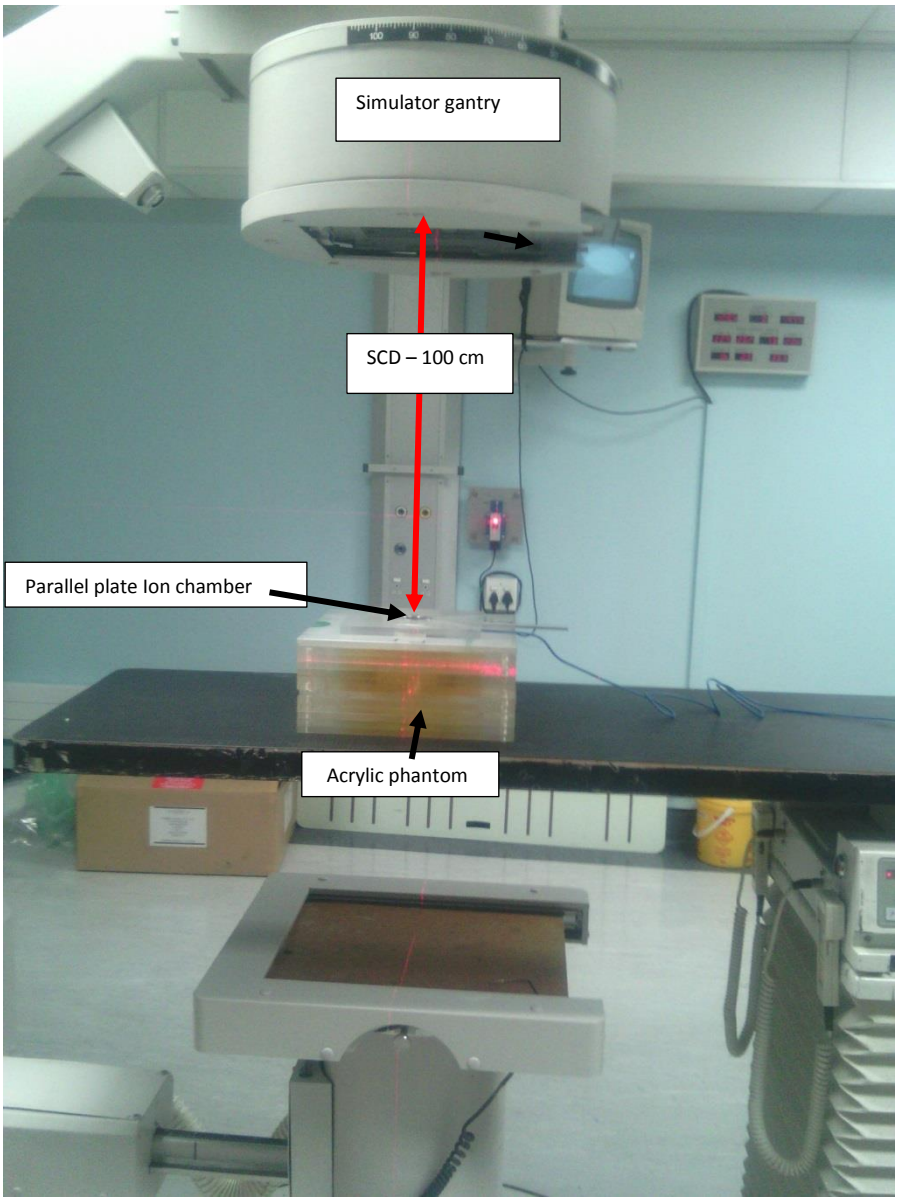

Fig. 18.The setup for measurements of radiographic dose on the radiotherapy simulator at CMJAH.

3.3.5 Patients imaging data collection procedure

20 patients who had completed radiation treatment were arbitrarily selected from each hospital during the period of 07 March 2017 to 31 May 2017. The imaging modalities and parameters used during planning and IGRT were collected from the electronic records. The following data was collected at the hospitals:

(a) CT (both at CMJAH and RBMI)

- Number of slices
- Slice thickness
- Number of CT examinations

(B) MV Portal imaging (CMJAH)

- Monitor units
- Frequency of imaging
- Field size
- Source to skin distance
- Number of projections

(c) Toshiba LX40 Simulator (CMJAH) and kV planar imager-Varian OBI (RBMI)

- kVp
- Exposure(mAs)
- Field size
- Focal to skin distance(FSD)
- Frequency of imaging
- Number of projections

CHAPTER 4

4. RESULTS AND DISCUSSION

4.1 In phantom dosimetry results

4.1.1 CT dose at CMJAH and RBMI

The CTDI results for the CT scanners used for treatment planning at each site are shown in Table 5.

Quantity	CMJAH		RBMI	
	Head	Body	Head	Body
$CTDI_{,PMMA,100,C}$(mGy)	17.68	12.92	66.89	17.29
$CTDI_{,PMMA,100,P}$(mGy)	18.12	23.93	78.46	38.89
$CTDI_{W}$ (mGy)	17.98 ± 1.45	20.26 ± 1.64	74.60 ± 6.19	31.69 ± 2.63
Pitch factor	1.00	1.00	0.94	0.94
$CTDI_{VOL}$ (mGy)	17.98 ± 1.45	20.26 ± 1.64	79.53 ± 6.60	33.79 ± 2.80

Table 5. CTDI results obtained at CMJAH and RMBI are shown. Measurements were made using 10 cm pencil type ionization chamber with a calibration coefficient traceable to the BIPM and an acrylic head and body phantom. The estimated relative expanded uncertainty of measurements was 8.1 and 8.3 (with k=2, corresponding to 95 % confidence level) for CMJAH and RBMI respectively.

The computed $CTDI_{vol}$ from $CTDI_{100}$ measurements were 17.98 ± 1.45 mGy for the head phantom and 20.26 ± 1.64 mGy for the body phantom at CMJAH, and 79.53 ± 6.60 mGy and 33.79 ± 2.80 mGy for head and body phantom respectively at RBMI. The average scan length from the planning CT at CMJAH was approximately 37 cm, whereas the average the scan length at RBMI was approximately 45 cm.

4.1.2 kVCBCT dose at RBMI

Indicated in table 6 are the kVCBT results measured at RBMI. Shown in table 7 is the comparison of kVCBT dose results measured by Hyer et al and dose results measured at RBMI.

Quantity	RBMI	
	Head	Body
$CTDI_{,PMMA,100,C}$ (mGy)	5.31	10.71
$CTDI_{,PMMA,100,P}$ (mGy)	5.14	16.25
$CTDI_{W}$ (mGy)	5.20 ± 0.43	14.40 ± 1.20
$_{n}CTDI_{w}$ (mGy/100mAs)	2.00 ± 0.16	1.40 ± 0.11

Table 6. kVCBCT dose results are shown. The dose was measured using the PTW-Freiburg TM77334 ionization chamber and acrylic head and body. The Uncertainty of measurements was 8.3, with k=2, corresponding to 95 % confidence level

	Elekta XVI kVCBCT		Varian OBI kVCBCT		Varian OBI kVCBCT	
Quantity	Hyer at al.		Hyer at al.		RBMI	
	Head	Pelvis	Head	Pelvis	Head	Pelvis
$_{n}CTDI_{w}$ (mGy/100mAs)	2.73	1.47	3.57	3.17	1.97	1.36
$CTDI_{w}$ (mGy)	0.98 ± 0.01	24.13 ± 0.08	5.17 ± 0.03	21.57 ±0.14	5.20 ±0.43	14.40 ± 1.19

Table 7. Comparison of the weighted and weighted-normalized cone beam CDTI values measured by Hyer et al.[40] on Elekta XVI and Varian OBI systems with the values measured at RBMI using a 16 cm and 32 cm diameter cylindrical phantom.

4.1.3 ESAK measurements on the Varian OBI kV planar imager

Table 8 indicates the ESAK measurements at RBMI on a Varian for a fixed field size of 20 × 20 cm^2 using the exposure parameter settings defined in the imaging protocol of the department. Different exposure parameters have been defined for different sizes of patients, categorized as small to extra-large (approximately 10 cm to 40 cm separation respectively) in order to obtain images of optimal quality.

Head			
Projection	Applied Voltage (kV)	Field size	ESAK (mGy)
AP	85	20 × 20 cm^2	0.31 ± 0.03
LAT	65	20 × 20 cm^2	0.12 ± 0.01
Pelvis AP			
Size	Applied Voltage (kV)	Field size	ESAK(mGy)
Small	75	20 × 20 cm^2	0.16 ± 0.01
Medium	75	20 × 20 cm^2	0.21 ± 0.02
Large	75	20 × 20 cm^2	0.27 ± 0.02
Extra large	75	20 × 20 cm^2	0.33 ± 0.03
Pelvis lateral			
Size	Applied Voltage (kV)	Field size	ESAK (mGy)
Small	120	20 × 20 cm^2	1.49 ± 0.13
Medium	120	20 × 20 cm^2	1.49 ± 0.13
Large	120	20 × 20 cm^2	3.18 ± 0.27
Extra large	120	20 × 20 cm^2	3.18 ± 0.27

Table 8. The ESAK results for Varian OBI kV planar imager. The measurements were made with the field size set to 20 × 20 cm^2, obtained with a PTW-Freiburg TM77334 parallel ionization chamber placed on a phantom at an SCD 0f 100 cm. The uncertainty of measurements was approximately 8.5 (with k=2, for 95 % confidence level).

4.1.4 ESAK on the Toshiba simulator at CMJAH

Shown in table 9 and 10 are ESAK measurements results obtained on the radiotherapy simulator at CMJAH. Table 9 indicates the variation of ESAK with voltage (kVp) and exposure (mAs). Table 10 indicates the ESAK normalized to mAs. The variation is shown in figure 16. Table 11 indicates ESAK measures for a fixed field size of 20 × 20 cm^2 and the exposure setting from the technique chart of the department. Similarly to RMBI, patients are categorized according to size as "average" to "big" on the technique chart with suggested exposure settings for obtaining images of acceptable quality.

Applied Voltage (kV)	ESAK (mGy)					
	100 mAs	80 mAs	50 mAs	40 mAs	20 mAs	10 mAs
50	1.547	1.251	0.728	0.614	0.296	0.136
60	2.495	2.019	1.248	0.975	0.476	0.227
70	3.513	2.896	1.751	1.392	0.673	0.314
80	4.735	3.828	2.373	1.880	0.918	0.448
90	6.143	4.972	3.099	2.430	1.204	0.647
100	7.504	5.982	3.752	2.958	1.457	0.728

Table 9. The ESAK results for the Toshiba radiotherapy simulator for a variety of exposure settings. The measurements were made with the field size set to 20 × 20 cm^2, obtained with a parallel ionization chamber placed on a 30 × 30 × 30 cm^3 acrylic phantom at an SCD of 100 cm.

Applied Voltage (kV)	ESAK (mGy/ mAs)
50	0.015 ± 0.001
60	0.024 ± 0.002
70	0.034 ± 0.003
80	0.047 ± 0.003
90	0.062 ± 0.005
100	0.074 ± 0.006

Table 10. The mean ESAK results, normalized to exposure (mAs) setting. The uncertainty of measurements was approximately 8.5 (with k=2, for 95 % confidence level).

Head				
Projection	mAs	Applied Voltage (kV)	Field size	ESAK (mGy)
AP	31.2	60	20 × 20 cm^2	0.76 ± 0.07
LAT	25.0	55	20 × 20 cm^2	0.49 ± 0.04

Pelvis AP				
Size	mAs	Applied Voltage (kV)	Field size	ESAK(mGy)
Average	40.0	63	20 × 20 cm^2	1.12 ± 0.09
Thin	31.2	60	20 × 20 cm^2	0.76 ± 0.07
Big	50.0	70	20 × 20 cm^2	1.72 ± 0.15

Pelvis lateral				
Size	mAs	Applied Voltage (kV)	Field size	ESAK (mGy)
Average	81.0	80	20 × 20 cm^2	3.78 ± 0.32
Thin	80.0	77	20 × 20 cm^2	3.24 ± 0.28
Big	100.0	96	20 × 20 cm^2	7.11 ± 0.60

Table 11. The ESAK for the imaging protocol at CMJAH is shown. The uncertainty of measurements was approximately 8.5 (with k=2, for 95 % confidence level).

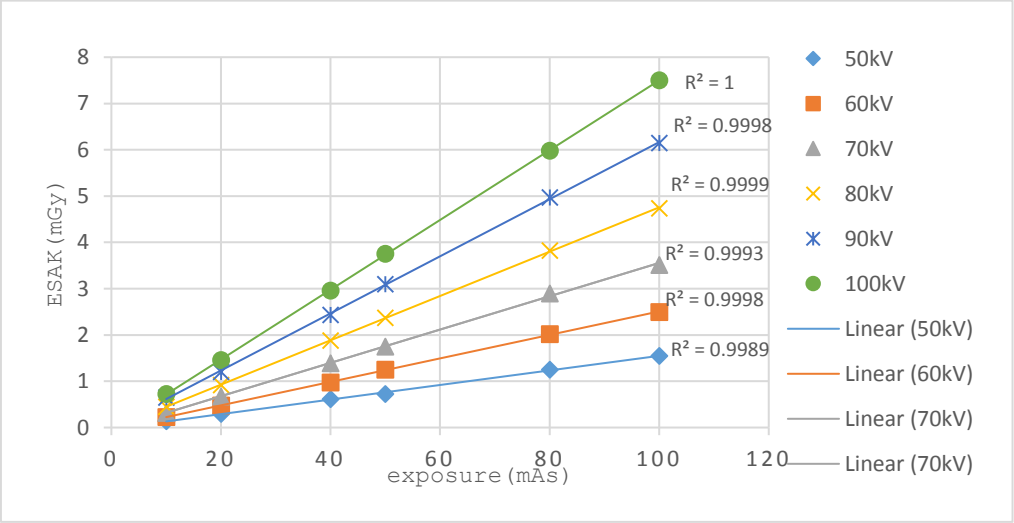

Fig. 16. A chart of results in table 8, indicating the variation of ESAK with mAs and tube potential (kVp) from measurement carried out on a Toshiba simulator at CMJAH is shown. The ESAK increases with increasing mAs and kVp. The regression coefficient of approximately 1, indicated the linear relationship between the ESAK and mAs.

4.2 Estimation of patient imaging dose at CMJAH

The dose results indicated in Tables 12-16 represent the imaging dose (absorbed dose to the isocentre and ESAK) accumulated from acquisition of simulation films, planning CT examinations and daily positional verifications on the treatment machine, respectively. The patient dose from fluoroscopic screening, acquisition of films during a High dose Rate (HDR) brachytherapy procedure (if relevant) or other imaging modalities such as Positron Emission tomography (PET) and any other diagnostic imaging during workup, have not been taken into account in this study.

4.2.1 Planning CT dose

Patient	No. of slices	Thickness (mm)	No. of CT exams	length (mm)	DLP (mGy · cm)
1	68	5	1	340	688.92
2	70	5	1	350	709.19
3	60	5	1	300	607.87
4	76	5	1	380	683.08
5	76	5	1	380	769.97
6	74	5	1	370	665.11
7	76	5	1	380	769.97
8	74	5	1	370	665.11
9	64	5	1	325	658.53
10	74	5	1	370	665.11
11	76	5	1	380	769.97
12	108	3	1	324	582.42
13	110	3	1	330	593.20
14	-	-	-	-	-
15	-	-	-	-	-
16	128	3	1	384	778.08
17	-	-	-	-	-
18	120	3	2	360	1294.26
19	118	3	2	354	1272.69
20	167	3	2	501	1801.18

Table 12. CT dose estimates of patients at CMJAH are shown. The total examination dose is presented as the dose length product (DLP), which is a product of the $CDTI_{vol}$ and the total scan length of the CT examination. Patients 14, 15 and 17 did not have planning CTs.

4.2.2 MV portal imaging dose to isocentre

Dual exposures were obtained consisting of a sequence of two exposures, with the first exposure being equivalent to the treatment field, followed by a larger rectangular field to localize the field within the surrounding anatomy. Table 13 indicates the dose results from first exposure and table 14 is the dose from larger open field. Higher monitor units (MU) are delivered for larger patients.

Patient number	AP/PA equivalent square field size cm	Output factor mu/cGy	Depth cm	MU	AP/PA Dose cGy	Lateral equivalent square field size cm	Output factor mu/cGy	Depth cm	MU	lateral Dose cGy
1	16	1.26	11.7	4	3.17	16	1.53	16.9	5	2.61
2	17	1.21	10.7	4	3.31	17	1.21	10.7	5	3.31
3	17	1.17	9.6	4	3.42	16	1.58	18.0	4	2.53
4	10	1.03	3.0	4	1.94	15	1.08	6.2	3	1.85
5	22	1.25	13.2	2	3.20	-	-	-	-	-
	20	1.27	13.2	4	3.15	-	-	-	-	-
6	19	1.14	9.0	4	1.75	19	1.48	16.8	3	1.35
	15	1.17	9.0	2	1.71	16	1.51	16.8	3	1.32
7	22	1.04	6.7	2	3.85	-	-	-	-	-
	19	1.06	6.7	4	1.89	-	-	-	-	-
8	18	1.20	10.7	2	1.67	17	1.51	17.2	3	1.32
9	17	1.16	9.2	2	1.72	16	1.52	17.2	3	1.32
10	17	1.26	12.0	2	1.59	18	1.47	16.3	3	1.36
11	17	1.34	13.7	2	1.49	16	1.53	17.3	3	1.31
12	10	1.12	6.3	3	2.68	10	1.13	6.3	2	2.65
13	11	0.99	1.9	3	3.03	11	0.99	1.9	2	3.03
	13	0.98	1.9	3	3.06	-	-	-	-	
14	17	1.18	10.3	3	2.54	15	1.85	21.5	5	2.16
15	17	1.09	7.3	2	1.83	17	1.40	15.1	3	1.43
16	10	1.32	10.8	2	1.52	10	1.69	17.0	3	1.18
17	12	1.25	10.0	3	2.40	12	1.25	10.0	4	2.40
18	11	1.02	3.2	3	2.94	11	1.01	3.2	2	2.97
19	15	1.15	8.3	3	2.61	17	1.13	8.7	3	2.65
20	13	1.47	15.1	2	1.36	13	1.47	15.1	3	1.36

Table 13. Portal imaging dose delivered to isocentre from the treatment field verifications of each patient.

Patient number	AP/PA equivalent square field size cm	Output factor mu/cGy	Depth cm	MU	AP/PA Dose cGy	Lateral equivalent square field size cm	Output factor mu/cGy	Depth cm	MU	lateral Dose cGy
1	28	1.18	11.7	5	4.24	28	1.38	16.9	5	3.62
2	29	1.15	10.7	5	4.37	29	1.15	10.7	5	4.35
3	29	1.12	9.6	5	4.48	29	1.42	18.0	4	2.82
4	16	0.98	3.0	3	3.06	21	1.04	6.2	3	2.90
5	26	1.23	13.2	3	2.44	-	-	-	-	-
	24	1.24	13.2	3	2.42	-	-	-	-	-
6	31	1.08	9.0	3	2.79	31	1.35	16.8	3	2.22
	15	1.17	9.0	3	2.56	16	1.52	16.8	3	1.97
7	34	1.02	6.7	5	4.90	-	-	-		
	19	1.07	6.7	3	2.80	-	-	-		
8	24	1.18	10.7	3	2.54	23	1.42	17.2	3	2.11
9	23	1.11	9.2	3	2.71	22	1.43	17.2	3	2.10
10	23	1.22	12.0	3	2.47	24	1.36	16.3	3	2.21
11	23	1.48	13.7	3	2.03	22	1.43	17.3	3	2.10
12	20	1.04	6.3	2	1.92	20	1.04	6.3	2	1.92
13	21	0.95	1.9	2	2.12	21	0.95	1.9	2	2.12
	13	0.98	1.9	4	4.08	-	-	-	-	
14	29	1.12	10.3	4	3.59	27	1.65	21.5	5	3.04
15	23	1.05	7.3	3	2.87	23	1.33	15.1	3	2.26
16	18	1.21	10.8	3	2.48	18	1.49	17.0	3	2.01
17	24	1.14	10.0	4	3.51	24	1.14	10.0	4	3.51
18	21	0.97	3.2	2	2.07	21	0.97	3.2	2	2.07
19	21	1.09	8.3	3	2.76	23	1.11	8.7	3	2.71
20	19	1.37	15.1	3	2.19	19	1.37	15.1	3	2.19

Table 14. Portal imaging dose from the second open field exposure used for verification.

Table 15 indicates the dose accumulated by patients during the complete course of treatment from dual exposures during MV portal imaging. The dose was calculated using the tabulated output factors for 6 MV, the equivalent square of the verification field was calculated in order to interpolate the output factor at the depth of interest. The total dose indicated was computed as the product of the calculated dose and the frequency of imaging. Portal imaging at CMJAH is typically done on the first day and half way through treatment, but the actual frequency of imaging collected from the Oncology information management system.

Patient number	No. of AP/PA verifications $N_{AP/PA}$	No. of lateral verifications $N_{lateral}$	Total dual exposure dose $T_{AP/PA}$ cGy	Total dual exposure dose $T_{lateral}$ cGy	$T_{AP/PA} + T_{lateral}$ cGy	Effective Dose AP/PA mSv	Effective Dose Lateral mSv	Total effective dose $T_{AP/PA} + T_{lateral}$ mSv
1	2	2	14.82	12.48	27.30	9.71	11.00	20.72
2	2	2	15.35	15.31	30.65	10.05	13.50	23.56
3	2	2	15.81	10.70	26.50	10.36	9.43	19.79
4	2	2	10.01	9.50	19.51	1.51	1.44	2.95
5	2	2	11.18	0.00	11.18	7.32	0.00	7.32
	1	1	5.57	0.00	5.57	3.65	0.00	3.65
6	2	2	9.09	7.15	16.24	3.89	2.88	6.78
	2	2	8.55	6.60	15.14	3.66	2.66	6.32
7	5	5	43.74	0.00	43.74	28.66	0.00	28.66
	5	5	23.45	0.00	23.45	15.37	0.00	15.37
8	3	3	12.63	10.31	22.94	8.27	9.09	17.37
9	2	2	8.88	6.83	15.71	5.82	6.02	11.84
10	2	2	8.11	7.13	15.25	5.32	6.29	11.61
11	3	2	10.58	6.81	17.39	6.93	6.01	12.94
12	2	2	9.20	9.16	18.36	1.39	1.38	2.78
13	3	3	15.44	15.44	30.88	2.33	2.33	4.67
	3		21.43	0.00	21.43	3.24	0.00	3.24
14	7	3	42.91	15.61	58.51	28.11	13.76	41.88
15	3	3	14.12	11.05	25.17	9.25	9.75	19.00
16	13	8	51.93	25.57	77.50	22.25	10.31	32.56
17	6	6	35.45	35.45	70.91	5.36	5.36	10.72
18	1	1	5.01	5.04	10.06	0.76	0.76	1.52
19	2	2	10.75	10.74	21.49	1.62	1.62	3.25
20	2	2	7.10	7.10	14.20	1.07	1.07	2.15

Table 15. The total dose to the isocentre from MV dual exposure portal imaging.

4.2.3 Simulator radiograph Entrance Surface Dose

The ESAK results measured on the radiotherapy simulator are indicated in table 16. The ESAK at the Focus Surface Distance (FSD) of each patient was calculated by applying the inverse square law to the measured ESAK and multiplied by the frequency of imaging.

Patient number	Lateral FSD (cm)	No. of exams	Lateral ESAK at FSD (mGy)	AP/PA FSD (cm)	No. of exams	AP/PA ESAK at FSD (mGy)
1	83.1	2	10.96	88.3	2	2.88
2	89.3	2	9.49	89.3	2	2.82
3	82.0	2	11.26	90.4	2	2.75
4	93.2	2	1.13	97.0	2	1.61
5	-		-	83.2	2	3.25
6	83.2	2	10.93	91.0	2	2.72
7	-		-	93.3	2	2.58
8	82.8	2	11.04	89.2	2	2.83
9	82.8	2	11.04	89.3	2	2.82
10	83.7	2	10.80	88.0	2	2.90
11	82.7	2	11.07	86.3	2	3.02
12	93.7	2	1.12	93.7	2	1.73
13	98.1	2	1.02	98.1	2	1.58
14	78.5	2	12.28	89.7	2	2.79
15	84.9	2	10.50	92.7	2	2.62
16	83.0	2	10.99	89.2	2	2.83
17	90.0	2	1.21	90.0	2	1.88
18	96.8	2	1.05	96.8	2	1.62
19	91.3	2	1.18	91.7	2	1.81
20	84.9	2	1.36	84.9	2	2.11

Table 16. The estimate of ESAK for patients at CMJAH delivered during radiographic planar imaging on a radiotherapy simulator is shown.

4.3 Estimation of the patient imaging dose at RBMI

The dose results indicated in table 17-19 represent the dose from the planning CT examination (DLP), daily positional verification on the treatment machine using kVCBCT (DLP) and kV portal imaging (ESAK) respectively.

4.3.1 Planning CT dose

Patient number	Number of slices	Slice thickness (mm)	Scan length (cm)	Number of CT exams	$CTDI_{VOL}$ (mGy)	DLP (mGy · cm)
1	134	3	40.2	1	79.53	3197.20
2	154	3	46.2	1	79.53	3674.40
3	73	3	21.9	1	79.53	1741.76
4	80	3	24.0	1	79.53	1908.78
5	66	3	19.8	1	79.53	1574.74
6	193	3	57.9	1	79.53	4604.93
7	154	3	46.2	1	33.79	1561.03
8	160	3	48.0	1	33.79	1621.85
9	151	3	45.3	1	33.79	1530.62
10	147	3	44.1	1	33.79	1490.07
11	154	3	46.2	1	33.79	1561.03
12	144	3	43.2	1	33.79	1459.67
13	162	3	48.6	1	33.79	1642.12
14	149	3	44.7	1	33.79	1510.35
15	248	3	74.4	1	33.79	2513.87
16	143	3	42.9	1	33.79	1449.53
17	154	3	46.2	1	33.79	1561.03
18	134	3	40.2	1	33.79	1358.30
19	185	3	55.5	1	33.79	1875.26
20	234	3	70.2	1	33.79	2371.96

Table 17. CT dose estimates of patients at RBMI are shown. The total dose is indicated by the dose length product (DLP), which is a product of the $CDTI_{vol}$ and the total scan length of the actual CT examination for each patient.

4.3.2 kVCBCT dose

Patient No.	Scan length (cm)	Measured $CTDI_w$ (mGy)	$_nCTDI_w$ (mGy /mAs)	Exposure (mAs)	Calculated $CTDI_w$ (mGy)	DLP (mGy·cm)	No. of CBCT exams (F)	DLP x F (mGy · cm)
1	17.6	5.20	0.02	145	2.85	50.12	7	350.84
2	17.4	5.20	0.02	145	2.85	49.78	5	248.90
3	17.6	5.20	0.02	145	2.85	50.18	4	200.72
4	17.6	5.20	0.02	145	2.85	50.29	5	251.45
5	17.6	5.20	0.02	145	2.85	50.12	7	350.84
6	17.6	5.20	0.02	145	2.85	50.12	6	300.72
7	15.9	14.40	0.01	1048	14.29	227.55	6	1365.30
8	15.8	14.40	0.01	1048	14.29	225.55	5	1127.75
9	15.7	14.40	0.01	1048	14.29	224.40	5	1122.00
10	15.8	14.40	0.01	1049	14.31	225.33	7	1577.31
11	15.9	14.40	0.01	1049	14.31	227.91	6	1367.46
12	15.8	14.40	0.01	997	13.60	214.57	6	1287.42
13	15.9	14.40	0.01	1049	14.31	227.48	2	454.96
14	15.9	14.40	0.01	1048	14.29	227.26	3	681.78
15	15.7	14.40	0.01	1049	14.31	224.47	2	448.94
16	15.9	14.40	0.01	1049	14.31	228.05	7	1596.35
17	15.7	14.40	0.01	1048	14.29	223.83	3	671.49
18	15.7	14.40	0.01	1046	14.27	224.55	3	673.65
19	16.2	14.40	0.01	1075	14.66	237.52	6	1425.12
20	16.0	14.40	0.01	1087	14.83	236.46	7	1655.22

Table 18. kVCBCT dose estimates of patients at RBMI are shown. The total dose is presented as the product of dose length product (DLP) and the total number of kVCBCT examinations. The DLP was calculated as the product of the $CDTI_{vol}$ and the total scan length of the CT examination.

4.3.3 kV portal imaging Dose

The ESAK at the FSD of each patient was calculated by applying the inverse square law to the measured ESAK assuming a fixed field size of 20 × 20 cm^2 for all patients. The total ESAK was computed as the product of calculated ESAK and the frequency on imaging. The kV portal imaging procedure at RBMI consists of a single exposure of an open rectangular localization field; dual exposures are not carried out.

Patient No.	Lateral FSD (cm)	No. of verifications	Lateral ESAK at FSD (mGy)	AP/PA FSD (cm)	No. of verifications	AP/PA ESAK at FSD (mGy)
1	83.4	7	1.16	88.2	7	2.79
2	91.5	5	0.69	91.1	6	2.24
3	91.8	6	0.82	88.4	6	2.38
4	87.6	2	0.30	87.4	2	0.81
5	92.7	7	0.94	90.8	7	2.63
6	97.9	7	0.85	98.0	7	2.26
7	83.9	5	22.56	89.7	5	1.69
8	77.6	4	9.93	89.4	4	1.07
9	83.7	4	18.13	92.5	4	1.27
10	80.6	7	16.10	87.4	8	2.23
11	78.5	4	20.61	87.3	4	1.42
12	83.4	11	23.63	89.9	10	2.64
13	80.3	5	24.62	89.3	5	1.34
14	82.2	4	18.80	88.2	3	1.05
15	82.8	3	13.90	88.9	3	1.25
16	83.4	7	31.96	89.8	7	2.36
17	81.2	3	14.45	80.2	3	1.27
18	82.1	3	14.13	88.8	3	1.03
19	68.4	6	40.72	90.5	6	2.41
20	80.0	7	34.73	86.3	7	3.10

Table 19. The calculated ESAK for kV planar portal imaging for both the anterior-posterior and lateral projections is shown.

4.4 Estimation of the total effective dose

The effective dose measurements were computed using equation 13. The DLP for both the CT and kVCBCT was converted into the effective dose by applying the conversion factors reported in table 3 of the AAPM task group 23[23]. The estimation of effective dose from 6 MV portal imaging was calculated using the conversion factors determined by Waddington and MacKenzie (their results are summarized in table X of the AAPM report Task group 75[15]). Their measurements were made at an SSD of 88 cm for a fixed field size of 18 × 15.6 cm^2. For the calculation of patient effective dose in this report, the inverse square law was applied to the results to correct for the difference in the actual patient SSD and the SSD used by Waddington and MacKenzie. The conversion factors for the estimation of effective dose from x-ray imaging were determined from JC Le Heron[32], as in table 1 and 2 of the publication.

4.4.1 Patient effective dose at CMJAH

Table 20-22 indicates the effective dose accumulated by patients during the complete course of treatment from MV portal imaging, acquisition of simulation films and planning CT examinations respectively. The results shown in table 21 do not take into account the dose received during fluoroscopic screening but only the dose resulting from acquisition of localization images for patient set up verification. Indicated in table 23 is the sum of total effective doses accumulated from the planning CT, simulator and MV portal imaging during the complete course of treatment.

The average effective dose to patients investigated at CMJAH from the planning CT, simulator and MV portal imaging for all imaging procedures carried out during their complete course of treatment was 7.53 ± 0.61 mSv, 0.37 ± 0.03 mSv and 15.53 ± 0.78 mSv respectively. On average, the effective dose per procedure was 7.57 ± 0.61 mSv, 0.19 ± 0.02 mSv and 4.80 ± 0.24 mSv for the planning CT, simulation and MV portal imaging respectively.

For imaging acquired during the complete course of treatment, the MV portal imaging dose contribution was the highest. The MV portal imaging dose was primarily influenced by the radiation beam collimation, and the frequency of imaging.

Patient No.	Total sum of AP/PA and lateral dose $T_{AP/PA} + T_{lateral}$ cGy	Total effective dose $T_{AP/PA} + T_{lateral}$ mSv
1	27.30	20.72 ± 1.05
2	30.65	23.59 ± 1.18
3	26.50	19.79 ± 0.99
4	19.51	2.95 ± 0.15
5	11.18	10.97 ± 0.55
6	16.24	13.10 ± 0.64
7	43.74	44.03 ± 2.20
8	22.94	17.37 ± 0.87
9	15.71	11.84 ± 0.59
10	15.25	11.61 ± 0.58
11	17.39	12.94 ± 0.65
12	18.36	2.78 ± 0.14
13	52.31	7.91 ± 0.40
14	58.51	41.88 ± 2.09
15	25.17	19.00 ± 0.95
16	77.50	32.56 ± 1.63
17	70.91	10.72 ± 0.54
18	10.06	1.52 ± 0.08
19	21.49	3.25 ± 0.16
20	14.20	2.15 ± 0.11
Average effective dose		15.53 ± 0.78

Table 20. Estimate of the effective dose resulting from 6 MV dual exposure verification carried out during the complete course of treatment.

Patient number	$N_{AP/PA}$	$N_{lateral}$	Effective Dose AP/PA mSv	Effective Dose Lateral mSv	Total effective dose $T_{AP/PA} + T_{lateral}$ mSv
1	2	2	0.20 ± 0.02	0.43 ± 0.04	0.63 ± 0.06
2	2	2	0.20 ±0.02	0.37 ± 0.03	0.57 ± 0.05
3	2	2	0.19 ±0.02	0.44 ± 0.04	0.63 ± 0.06
4	2	2	0.01 ±0.00	0.01 ± 0.001	0.02 ± 0.00
5	2	-	0.23 ±0.02	-	0.23 ± 0.02
6	2	2	0.19 ±0.02	0.42 ± 0.04	0.61 ± 0.06
7	2	-	0.18 ±0.02	-	0.18 ± 0.02
8	2	2	0.20 ± 0.02	0.43 ± 0.04	0.63 ± 0.06
9	2	2	0.20 ± 0.02	0.43 ± 0.04	0.63 ± 0.06
10	2	2	0.21 ± 0.02	0.42 ± 0.04	0.63 ± 0.06
11	2	2	0.21 ± 0.02	0.43 ± 0.04	0.64 ± 0.06
12	2	2	0.01 ± 0.00	0.01± 0.00	0.02 ± 0.02
13	2	2	0.01 ± 0.00	0.01 ± 0.00	0.02 ± 0.02
14	2	2	0.20 ± 0.02	0.48 ± 0.04	0.68 ± 0.06
15	2	2	0.19 ± 0.02	0.41 ± 0.04	0.6 ± 0.06
16	2	2	0.20 ± 0.02	0.43 ± 0.04	0.63 ± 0.06
17	2	2	0.01 ± 0.00	0.01 ± 0.00	0.02 ±0.00
18	2	2	0.01 ±0.00	0.01 ± 0.00	0.02 ± 0.00
19	2	2	0.01 ± 0.00	0.01 ± 0.00	0.02 ± 0.00
20	2	2	0.02 ± 0.00	0.01 ± 0.00	0.03 ± 0.00

Table 21. Estimate of the effective dose for each patient from radiotherapy simulator imaging.

Patient	No. of slices	Thickness (mm)	No. of CT exams	length (mm)	DLP (mGy · cm)	Effective dose (mSv)
1	68	5	1	340	688.92	10.33 ± 0.84
2	70	5	1	350	709.19	10.64 ± 0.86
3	60	5	1	300	607.87	9.12 ± 0.74
4	76	5	1	380	683.08	2.12 ± 0.17
5	76	5	1	380	769.97	11.55 ± 0.94
6	74	5	1	370	665.11	9.98 ± 0.81
7	76	5	1	380	769.97	11.55 ± 0.94
8	74	5	1	370	665.11	9.98 ± 0.81
9	64	5	1	325	658.53	9.88 ± 0.80
10	74	5	1	370	665.11	9.98 ± 0.81
11	76	5	1	380	769.97	11.55 ± 0.94
12	108	3	1	324	582.42	1.81 ± 0.15
13	110	3	1	330	593.20	1.84 ± 0.15
14	-	-	-	-	-	-
15	-	-	-	-	-	-
16	128	3	1	384	778.08	11.67 ± 0.95
17	-	-	1	-	-	-
18	120	3	2	360	1294.26	4.01 ± 0.32
19	118	3	2	354	1272.69	3.95 ± 0.32
20	167	3	2	501	1801.18	5.58 ± 0.45

Table 22. Estimate of the effective dose for each patient from the planning CT.

Patient number	CT effective dose (mSv)	Simulator effective dose (mSv)	6 MV portal imaging effective dose (mSv)	Total effective dose (mSv)
1	10.33 ± 0.84	0.63 ± 0.06	20.72 ± 1.04	31.68 ± 1.93
2	10.64 ± 0.86	0.57 ± 0.05	23.59 ± 1.18	34.77 ± 2.09
3	9.12 ± 0.74	0.63 ± 0.06	19.79 ± 0.99	29.54 ± 1.78
4	2.12 ± 0.17	0.02 ± 0.02	2.95 ± 0.15	5.09 ± 0.32
5	11.55 ± 0.94	0.23 ± 0.02	10.97 ± 0.55	22.75 ± 1.50
6	9.98 ± 0.81	0.61 ± 0.06	13.10 ± 0.66	23.69 ± 1.52
7	11.55 ± 0.94	0.18 ± 0.02	44.03 ± 2.20	55.76 ± 3.15
8	9.98 ± 0.81	0.63 ± 0.06	17.37 ± 0.87	27.98 ± 1.73
9	9.88 ± 0.80	0.63 ± 0.06	11.84 ± 0.59	22.35 ± 1.45
10	9.98 ± 0.81	0.63 ± 0.06	11.61 ± 0.58	22.22 ± 1.44
11	11.55 ± 0.94	0.64 ± 0.06	12.94 ± 0.65	25.13 ± 1.64
12	1.81 ± 0.15	0.03 ± 0.00	2.78 ± 0.14	4.61 ± 0.29
13	1.84 ± 0.15	0.03 ± 0.00	7.91 ± 0.40	9.77 ± 0.55
14	-	0.68 ± 0.06	41.88 ± 2.09	42.56 ± 2.15
15	-	0.60 ± 0.06	19.00 ± 0.95	19.60 ± 1.00
16	11.67 ± 0.95	0.63 ± 0.06	32.56 ± 1.63	44.86 ± 2.63
17	-	0.03 ± 0.00	10.72 ± 0.54	10.74 ± 0.54
18	4.01 ± 0.32	0.03 ± 0.00	1.52 ± 0.08	5.55 ± 0.40
19	3.95 ± 0.32	0.03 ± 0.00	3.25 ± 0.16	7.22 ± 0.48
20	5.58 ± 0.45	0.03 ± 0.00	2.15 ± 0.11	7.76 ± 0.56
Average effective dose	7.53 ± 0.61	0.37 ± 0.03	15.53 ± 0.78	22.68 ± 1.42

Table 23. Total effective dose estimates accumulated at CMJAH for each patient during a complete course of treatment resulting from the planning CT, simulation and 6 MV portal imaging.

4.4.2 Patient effective dose at RBMI

The results in table 24 represent the total effective dose accumulated from the planning CT, and daily positional verifications on the linear accelerator using kVCBCT and kV planar imaging during the complete course of treatment.

Patient number	CT effective dose (mSv)	kVCBCT effective dose(mSv)	kV portal effective dose (mSv)			Sum of effective doses from all modalities (mSv)
			AP/PA	Lateral	Total effective dose	
1	9.91 ± 0.82	1.09 ± 0.09	0.02	0.01	0.03 ± 0.00	11.03 ± 0.92
2	11.39 ± 0.95	0.77 ± 0.06	0.01	0.01	0.02 ± 0.00	12.18 ± 1.01
3	3.66 ± 0.30	0.42 ± 0.03	0.01	0.01	0.02 ± 0.00	4.10 ± 0.34
4	4.01 ± 0.33	0.53 ± 0.04	0.01	0.00	0.01 ± 0.00	4.55 ± 0.38
5	3.31 ± 0.27	0.74 ± 0.06	0.02	0.01	0.03 ± 0.00	4.08 ± 0.34
6	14.28 ± 1.19	0.93 ± 0.08	0.02	0.01	0.03 ± 0.00	15.24 ± 1.26
7	23.42 ± 1.94	20.48 ± 1.7	1.22	1.19	2.41 ± 0.20	46.31 ± 3.85
8	24.33 ± 2.02	16.92 ± 1.40	0.47	0.45	0.92 ± 0.08	42.17 ± 3.50
9	22.96 ± 1.91	16.83 ± 1.40	0.98	0.95	1.93 ± 0.16	41.72 ± 3.47
10	22.35 ± 1.86	23.66 ± 1.96	0.81	0.78	1.59 ± 0.14	47.60 ± 3.95
11	23.42 ± 1.94	20.51 ± 1.70	0.98	0.95	1.93 ± 0.16	45.86 ± 3.81
12	21.89 ± 1.82	19.31 ± 1.60	1.25	1.23	2.48 ± 0.21	43.68 ± 3.63
13	24.63 ± 2.04	6.82 ± 0.57	1.21	1.19	2.40 ± 0.20	33.85 ± 2.81
14	22.66 ± 1.88	10.23 ± 0.85	0.98	0.95	1.93 ± 0.16	34.82 ± 2.89
15	37.71 ± 3.13	6.73 ± 0.56	0.75	0.71	1.46 ± 0.12	45.90 ± 3.81
16	21.74 ± 1.80	23.95 ± 1.99	1.69	1.66	3.36 ± 0.29	49.05 ± 4.08
17	23.42 ± 1.94	10.07 ± 0.84	0.74	0.71	1.46 ± 0.12	34.95 ± 2.90
18	20.37 ± 1.69	10.10 ± 0.84	0.03	0.00	0.03 ± 0.00	31.93 ± 2.53
19	28.13 ± 2.33	21.38 ± 1.77	1.46	1.43	2.89 ± 0.25	52.40 ± 4.25
20	35.58 ± 2.95	24.83 ± 2.06	1.70	1.66	3.36 ± 0.29	63.77 ± 5.30
Average effective dose	19.96 ± 1.66	11.82 ± 0.98			1.49 ± 0.12	33.26 ± 2.76

Table 24. Total effective dose estimation to patients at RBMI from the planning CT, and kVCBCT and kV portal imaging accumulated during the complete course of treatment.

Accumulated effective dose from other imaging modalities such as PET scans used for image fusion, are not taken into account. The average effective dose from the planning CT, kVCBCT and kV portal imaging for all imaging procedures carried out during the complete course of treatment was 19.96 ± 1.66 mSv, 11.81 ± 0.98 mSv and 1.49 ± 0.12 mSv respectively. The kV portal imaging dose measured at RBMI ranged from 0.1 to 3.2 mGy. The greatest contribution to the total effective dose from imaging alone originated from the planning CT scan.

5. CONCLUSION

The results indicate that considerable dose could be delivered to patients during image guided radiotherapy, primarily when imaging procedures are over utilized and not optimized, adding more burden of dose to the already high levels of dose they receive from their treatment. The dose contribution from the planning CT was the highest in this study and was primarily influenced by the scan length. This can be reduced if scans are not acquired significantly beyond the ROI required for planning purposes. However, insufficient scan lengths may not provide sufficient image information required for radiation therapy planning.

Modern imaging techniques such as kVCBCT applied during patient setup verification, can also add a significant dose when over utilized.

In comparison with MV portal imaging dose, kV portal imaging dose is less and in some instances, more useful image quality can be obtained compared to MV imaging. The ability to simply subtract the MV portal imaging dose from the prescribed dose when imaging actual treatment ports should be considered when a large number of verifications are requested.

Imaging dose in IGRT should consider the ALARA principle without compromising the image quality and information required to achieve the objectives of IGRT. This requires optimization of beam collimation, exposure parameters for both types of portal imaging, as well as the prescribed frequency of imaging and the scan lengths for CT exams.

It is recommended that radiotherapy institutions examine the effective dose to patients from their IGRT modalities and adapt their imaging protocols accordingly. Given that CT doses were found to be the highest, it is highly recommended that institutions considering daily CBCT imaging and emerging advanced techniques using 4-dimensional CT for instance, pay due attention to the additional dose burden to patients.

6. REFERENCES

1. Bradley, WG. (2008). History of Medical Imaging. Proceedings of the American Philosophical Society, 152(3), 349-361. [online] Available at: http://www.jstor.org/stable/40541591 [Accessed 8 Jan. 2017].

2. Donaldson, R., and Kirk, B. (Eds.). (1995). A Periodical of Particle Physics. Beam line, 25(2). Retrieved March 8, 2016, from http://www.slac.stanford.edu/pubs/beamline/pdf/95ii.pdf

3. Sgantzos, M., et al. (2014). The physician who first applied radiotherapy, Victor Despeignes, on 1896. Hellenic Journal of Nuclear Medicine, 17(1), 45-46.

4. Berman,B. (2017. From Infrared to X-rays, the curious History of insible light. [Online] Available at: https://books.google.co.za/books?id=5sIgDgAAQBAJ&pg=PT94&lpg=PT94&dq=history+of+x+rays+Dr+W.+Gage+nebraska&source=bl&ots=chZmLcZp03&sig=GnSHf-BhtP3PUuzsSZYLOlrj3EA&hl=en&sa=X&ved=0ahUKEwi2pNK0wePYAhXKKsAKHTdGAeoQ6AEIMjAB#v=onepage&q&f=false [Accessed 19 Feb. 2016].

5. Developments in medical imaging – timeline. (n.d.). [Online] Available at: https://www.sciencelearn.org.nz/resources/1906-developments-in-medical-imaging-time [Accessed 19 Feb. 2016].

6. Society of Nuclear Medicine and Molecular Imaging (SNMMI. (n.d.). [Online] Available at: http://snmmi.files.cms-plus.com/docs/hist_corner_11_03.pdf [Accessed 19 Feb. 2016].

7. Khan, FM. (2003). The physics of radiation therapy. 3rd ed. Lippincott Williams & Wilkins, Philadelphia.

8. Aird, EG. (2004). Second cancer risk, concomitant exposures, and IRMER (2000). Br. J. Radiol. 77, pp.983–985.

9. NCRP Report No. 160: Ionizing Radiation Exposure of the Population of the United States. (2009). Journal of Radiological Protection, 29(3), pp.465-465.

10. NCRP Report No. 93: Ionizing Radiation Exposure of the Population of the United States. (1987). Journal of Radiological Protection.

11. Unscear.org. (2017). UNSCEAR 2008 report - Vol. I: Sources. [Online] Available at: http://www.unscear.org/unscear/en/publications/2008_1.html [Accessed 15 March. 2017].

12. Unscear.org. (2017).Radiation Booklet. [Online] Available at: http://www.unscear.org/unscear/en/publications/booklet.html [Accessed 25 Oct. 2017].

13. Podgorsak, E. (2005). Radiation Oncology Physics: A Handbook for Teachers and Students. 1st ed. Vienna: International Atomic Energy Agency.

14. Dhull, DA. (1970). Regional Cancer Centre Rohtak. [Online] Available at: http://rcc-rohtak.blogspot.co.za/2007/10/academic-event-with-us-ambassador.html [Accessed 22 Apr. 2016].

15. Murphy, MJ., et al. (2007). The management of imaging dose during image-guided radiotherapy: Report of AAPM Task Group 75. Medical Physics, Vol. 34, No. 10.

16. Islam, M., et al. (2006). Patient dose from kilovoltage cone beam computed tomography imaging in radiation therapy. Medical Physics, 33(6Part1), pp.1573-1582.

17. Ding, GX., et al. (2007). Characterization of kilovoltage x-ray beams for cone beam computed tomography in radiation therapy. Phys. Med Biol. 52, PP.1595-1615.

18. Kim, S., et al. (2011). Computed Tomography Dose index and Dose length product for cone beam CT: Monte Carlo simulation of a commercial system. J Appl Clin Med Phys. 12(2), pp.3395.

19. Scandurra, D., et al. (2014). A dosimetry technique for measuring kilovoltage cone-beam CT dose on a linear accelerator using radiotherapy equipment. J Appl Clin Med Phys. Vol 15. No.4

20. Morin, O., et al. (2007). Dose calculation using Megavoltage Cone Beam Computed Tomography. Int. J Radiation Oncology Biol Phys. 67.

21. Ding GX., et al. (2008). Accurate patient dosimetry of kilovoltage cone-beam CT in radiation therapy. Med Phys. 35, pp.1135-44.

22. Montanari, D., et al. (2014). Comprehensive evaluations of cone-beam CT dose in image guided radiation therapy via GPU-based Monte Carlo simulations. Phys Med Biol. 59(5), pp.1239-53.

23. McCollough, C., et al. (2008). The Measurement, Reporting, and Management of Radiation Dose in CT; Report No. 96 of AAPM Task Group 23.

24. Dixon, RL., et al. Comprehensive methodology for the evaluation of radiation dose in x-ray computed tomography: the future of CT dosimetry; Report of AAPM Task Group 111.

25. Robert Chu, YL., et al. (1991). Standardized methods for measuring diagnostic x-ray exposures; Report No. 31 of AAPM Task Group 8.

26. Shope, TB., et al.(1981). A method for describing the doses delivered by transmission x-ray computed tomography. MedPhys. 8, pp.488-95.

27. McCollough, CH., et al. (1999). Performance evaluation of a multislice CT system. Med. Phys. 26, pp. 2223–2230.

28. International Atomic Energy Agency. (2007). Dosimetry in Diagnostic Radiology: An International Code of Practice,Technical Reports Series No. 457, IAEA, Vienna

29. Bauhs, JA., et al. (2008). CT Dosimetry: Comparison of Measurement Techniques and Devices. RadioGraphics, 28(1), 245-253. doi:10.1148/rg.281075024

30. Dance, D., and Carlsson, G. (2007). 4. A HandbooK of Radiotherapy Physics: Theory and Practice (pp. 57-74). Boca Raton, Florida: Taylor & Francis Group, LLC.

31. Jacobi, W. (1975). The Concept of the Effective Dose – A Proposal for the Combination of Organ Doses, Rad. and Environm. Biophys. Vol.12, pp.101-109.

32. Heron, J. (1992). Estimation of effective dose to the patient during medical X-ray examinations from measurements of the dose-area product. Physics in Medicine and Biology, 37(11), pp.2117-2126.

33. McCollough, C., and Schueler, B. (2000). Calculation of effective dose. Med. Phys 27, pp. 828–37.

34. Pyone, Y., et al. (2017). Determination of effective doses in image-guided radiation therapy system.

35. Shrimpton, P. and Wall, B. (2009). Effective Dose and Dose-Length Product in CT. Radiology, 250(2), pp.604-605.

36. A Guide for the submission of initial reports on diagnostic x-ray systems and their major components. (1978). Rockville, Md.: U.S. Dept. of Health, Education, and Welfare, Public Health Service, Food and Drug Administration, Bureau of Radiological Health, Division of Compliance, X-Ray Products Branch.

37. Bipm.org. (2017). BIPM - About the BIPM. [Online] Available at: https://www.bipm.org/en/about-us [Accessed 6 Aug. 2016].

38. www.leucht.de, w. (2017). PTW: Acrylic and RW3 Slab Phantoms. [Online] Ptw.de. Available at: http://www.ptw.de/acrylic_and_rw3_slab_phantoms0.html [Accessed 12 Jul. 2016].

39. www.leucht.de, w. (2017). PTW: Acrylic and RW3 Slab Phantoms. [Online] Ptw.de. Available at: http://www.ptw.de/1852.html?&cId=190 [Accessed 12 Jul. 2016].

40. Hyer, D., et al. (2010). An organ and effective dose study of XVI and OBI cone beam CT systems. Journal of Applied Clinical Medical Physics, 11(2), pp.181-197

41. Alaei, P., Ding, G. and Guan, H. (2009). Inclusion of the dose from kilovoltage cone beam CT in the radiation therapy treatment plans. Medical Physics, 37(1), pp.244-248.

42. Serhal, BC., et al.(2001). Absorbed doses from spiral CT and conventional spiral tomography: a phantom vs cadaver study. Clin Oral Impl Res.

43. Wen, N., et al.(2006). Dose delivered from Varian's CBCT to patients receiving IMRT for prostate cancer. Phys. Med. Biol. 52.

44. Herman, M., et al. (2001). Clinical use of electronic portal imaging: Report of AAPM Radiation Therapy Committee Task Group 58. Medical Physics, 28(5), pp.712-737.

45. Sawyer, LJ., et al. (2009). Estimation of organ and effective doses resulting from cone beam CT imaging for radiotherapy treatment planning. Br J Radiol 82, pp. 577-584.

46. Pyone, Y., et al. (2017). Determination of effective doses in image-guided radiation therapy system.